VSB TECHNICAL UNIVERSITY OF OSTRAVA | FACULTY OF CIVIL ENGINEERING

22. ročník mezinárodní konference

Modelování v mechanice 2024

23. - 24. 5. 2024

Sborník rozšířených abstraktů

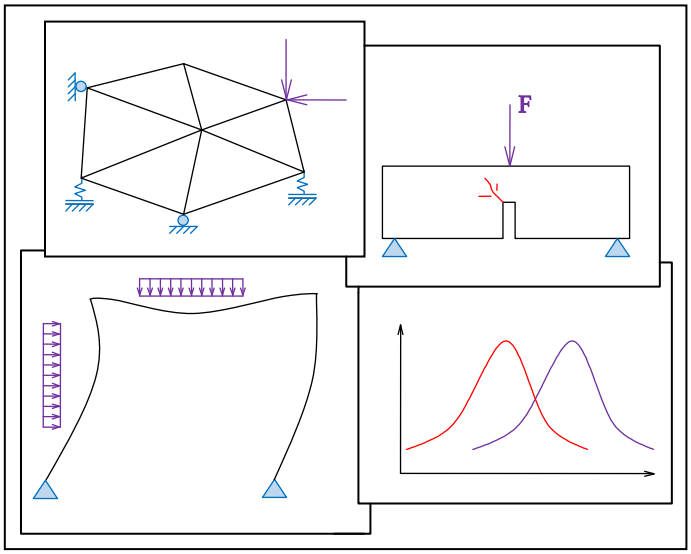

22nd International Conference

Modelling in Mechanics 2024

23rd and 24th May 2024

Proceedings of extended abstracts

ISBN 978-80-248-4735-1 (Print)
ISBN 978-80-248-4736-8 (Online)

TABLE OF CONTENTS / OBSAH

Verification of Stress State in the Lower Part of Steel Bridge Detail

Jiri BROZOVSKY[1], *Martin KREJSA*[1]

[1]VSB – Technical University of Ostrava, Faculty of Civil Engineering
17. Listopadu 15, Ostrava, Czech Republic

jiri.brozovsky@vsb.cz, martin.krejsa@vsb.cz

This contribution studies a stress state in a detail of the tension flange of the stringer at the point of connection of the cross member in the steel part of the steel-concrete bridge. Obtained results are used as basis for decision on use of simplified analytical approach for investigation of fatigue behaviour of the studied detail. The presented detail is based on a real steel bridge which is a part of highway system in Slovakia. The computational model was created with use of the uFEM software developed at the VSB-TUO.

The bridge was modelled as an linear elastic problem because the global stress state of the bridge should we in the elastic range. The model of the studied part of the bridge is shown in Fig. 1. An isoparametric 8-node finite element are used. The boundary conditions were set up to simulate effects of the rest of the bridge on the element. Their parameters were defined on basis of a global analysis of a beam model of the bridge. Material properties were defined asl linear elastic, as mentioned above. The steel was considered with the Young modulus E= 210 GPa and concrete with E= 37.7 GPa.

The load case studied here was an extreme load located over the center of the detail. Other cases were studied and this one was considered the most influential.

In the studied case if was shown that stresses in the studied part are rather slow for x and y direction but magnitudes higher for the z direction. Thus the assumption that x and y stresses can be omitted in simplified calculations was assessed as the valid one.

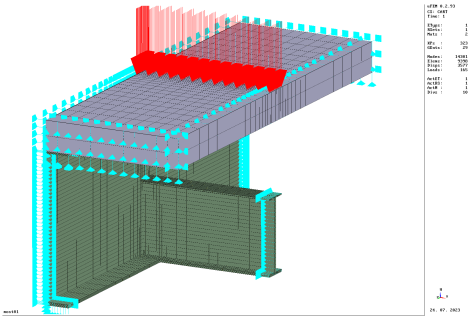

Fig. 1: Computational model of the structure.

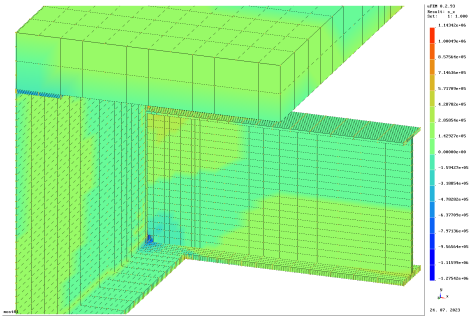

Fig. 2: Distribution of σ_x stresses (perpendicular to bridge axis).

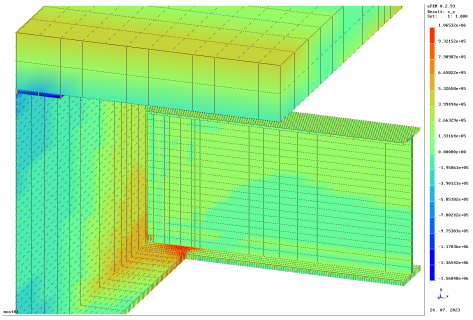

Fig. 3: Distribution of σ_z stresses (along bridge axis).

Acknowledgements

This contribution has been developed as a part of the research project of the Czech Science Foundation 21-14886S "Influence of material properties of high strength steels on durability of engineering structures and bridges".

Validation of a Numerical Model of MNC Connections Based on Experimental Data

Pavel DOBEŠ[1], *Marek JOHANIDES*[1], *Antonín LOKAJ*[2], *David MIKOLAŠEK*[2]

[1] Centre for Building Experiments and Diagnostics, Faculty of Civil Engineering, VSB – Technical University of Ostrava

[2] Department of Structures, Faculty of Civil Engineering, VSB – Technical University of Ostrava

pavel.dobes1@vsb.cz

The paper deals with the experimental and numerical analysis of MNC (=Multiple Nail Connectors) connections in timber, where slotted-in steel plates with double-sided welded nails of rectangular cross-section are used. Plates are pressed between two parts of the timber element.

Several variants of MNC connections were selected for testing, they differed in the used timber - KVH structural timber (ST) of C24 grade, glued laminated timber (GLT) of GL24h grade and laminated veneer lumber (LVL) Ultralam-R. Nine specimens of cross-sectional dimensions twice 75/160 mm were tested in tension parallel to the grain (∥) and nine specimens of cross-sectional dimensions twice 75/200 mm with the use of an external steel structure were tested in tension perpendicular to the grain (⊥) until failure under monotonic quasi-static loading. Slotted-in plates with a thickness of 10 mm were made of structural steel of S355J2G3 grade. Double-sided welded nails with a rectangular cross-section of 3/4 mm and a length of 50 mm had a minimum strength of 600 MPa. Continuous recording of the time, the tensile force and the deformation of the connection (load-deformation curves) was carried out during the test according to the EN 26891 standard. The experimental data were subsequently used to validate the numerical model of the selected variant.

The maximum load-carrying capacities (average values) for the individual tested variants were:
ST-∥ = 157.2 kN; GLT-∥ = 161.3 kN; LVL-∥ = 213.0 kN;
ST-⊥ = 138.9 kN; GLT-⊥ = 153.6 kN; LVL-⊥ = 167.5 kN.

The connections were broken after significant plastic deformation of the nails in the embedded timber. The nails were pulled out of the timber element while it was being opened. Nails were also torn off at the weld in some cases. Due to the uniform distribution of slender nails, the connection showed a high ductility before failure.

A beam-shell numerical model was created in the SCIA Engineer software to compare the experimental data (GLT-⊥). The numerical model considered orthotropy, slip modulus of connections, contact, material and geometric nonlinearities. The debugged model was in a good agreement with the experimental data (see Fig. 1).

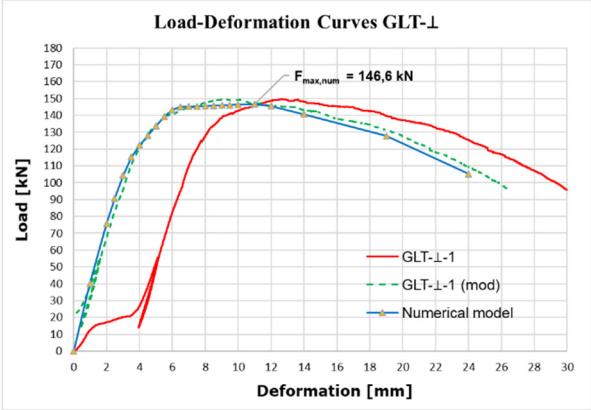

Fig. 1: Comparison of experimental and numerical curves

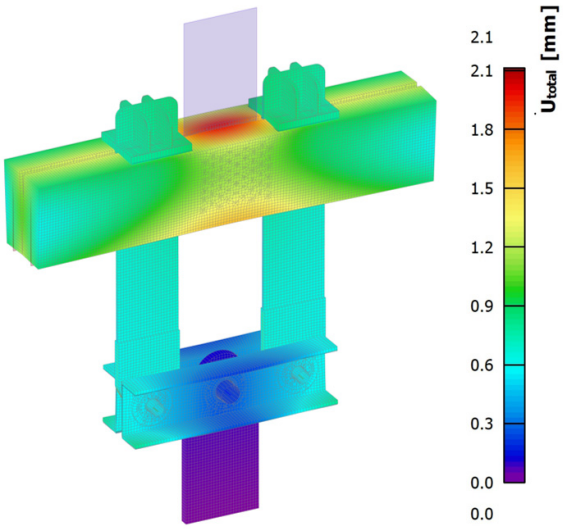

Fig. 2: Local deformation of the timber element (for $F_{max,num}$)

Acknowledgements

Financial support from VSB-Technical University of Ostrava, The Faculty of Civil Engineering, by means of the operating costs of The Department of Structures is gratefully acknowledged.

EVALUATION OF THE INFLUENCE OF ADMIXTURES ON THE CEMENT HYDRATION PROCESS IN 3D PRINTED CONCRETE

Karol FEDEROWICZ[1], Krzysztof CENDROWSKI[1], Pawel SIKORA[1]

[1]Faculty of Civil and Environmental Engineering, West Pomeranian University of Technology in Szczecin, Al. Piastów 50a, 70-311 Szczecin, Poland

kfederowicz@zut.edu.pl, krzysztof.cendrowski@zut.edu.pl, psikora@zut.edu.pl

The carbon footprint associated with concrete production is a significant environmental concern, highlighting the importance of research into sustainable additives. 3D printed concrete presents unique opportunities for reducing this footprint by optimizing material usage and integrating eco-friendly alternatives. Incorporating biochar and fines from recycled concrete as partial replacements for cement not only contributes to waste reduction but also helps mitigate the carbon emissions associated with traditional cement production. Biochar, derived from organic waste materials, acts as a carbon sink by sequestering carbon and reducing the overall embodied carbon content of the concrete mix. Similarly, the use of recycled concrete fines reduces the demand for raw materials, thereby lowering the environmental impact associated with quarrying and transportation.

This research aims to quantify the impact of incorporating biochar and concrete fines as partial replacements for cement on the hydration process and early-age strength development in 3D printed concrete. An optimized reference mixture was designed to fulfill specific requirements associated with 3D printing, including pumpability, extrudability, buildability, and open time. Four different levels of cement replacement were selected for investigation: 1.25%, 2.5%, 5%, and 10% by volume. Other materials such as silica fume, fly ash, water, superplasticizer, and sand remained constant.

The influence of biochar and concrete fines on strength development was determined after 1, 3, and 7 days. The hydration process was evaluated using an isothermal calorimeter on cement paste (with constant aggregate content in all mixes). To assess the influence of additives on rheological properties, the development of static yield stress over time was evaluated based on the methodology outlined in Figure 1. Additionally, flow table tests and mechanical property assessments (including dynamic modulus of elasticity development, shrinkage, and green strength) were conducted for each designed mixture. Figure 2 illustrates the influence of replacing cement with concrete fines on the development of dynamic modulus of elasticity.

This comprehensive study provides insights into how biochar and recycled concrete fines can be effectively utilized in 3D printed concrete formulations to enhance sustainability without compromising performance. The findings contribute to advancing environmentally friendly construction practices and optimizing the use of recycled materials in innovative construction technologies.

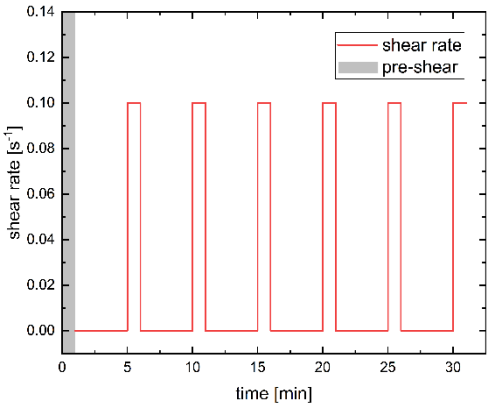

Fig. 1: Methodology of static yield stress determination test.

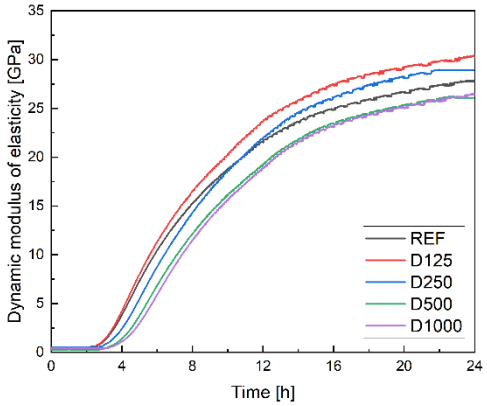

Fig. 2: Development of dynamic modulus of elasticity.

Acknowledgements

This research was funded in whole by the National Science Centre, Poland within Project No. 2022/45/N/ST8/01277 (PRELUDIUM-21).

USABILITY OF 3D PRINTING IN CONSTRUCTION INDUSTRY

Dominik GŘEŠICA[1], *David JURAČKA*[1], *Petr LEHNER*[1], *Martin KREJSA*[1]

[1] Department of Structural Mechanics, Faculty of Civil Engineering, VSB-Technical University of Ostrava, Ludvika Podeste 1875/17, 708 00 Ostrava-Poruba, Czech Republic

dominik.gresica.st@vsb.cz, david.juracka@vsb.cz, petr.lehner@vsb.cz, martin.krejsa@vsb.cz

In recent years and decades, the construction industry has been faced with new challenges and tasks that need to be solved with new technologies and approaches. One such approach is 3D printing [1]. It all starts with a 3D model, thanks to which the printing equipment gradually transforms the shape into the final form. It can use materials such as concrete, metal or polymers to create a 3D structure [2]. The technology of applying cement mixtures using robotic arms or gantry systems has been known for almost 15 years and is gaining ground in many forms.

On the other hand, the usability of 3D printing from metal or polymer-based material for structural load-bearing purposes is not widely represented and is a topic that has not been explored much. A smaller number of research teams focused on the use of 3D printing of metal materials for joints, where the goal is to optimize topologies or to focus on non-traditional architectural shapes [3].

An interesting possibility is the application of 3D printing to known and problematic details such as the joints of structures that do not have to have a repeating shape, for example membranes. Membrane or rope constructions generally present a challenge in the need to prepare the ideal inclination, shape or size of the connection at high tensile forces. This direction is explored in this paper both at a scale suitable for small 3D printers (see Fig. 1) and at a scale suitable for large 3D printers (see Fig. 2).

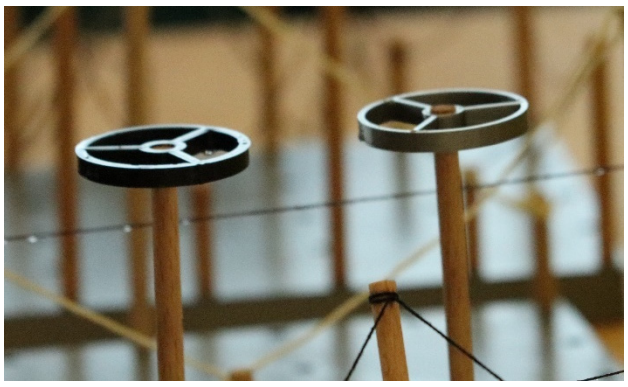

Fig. 1: Prototype of joint of the membrane to the support element made using 3D printing in scale approx. 1:100.

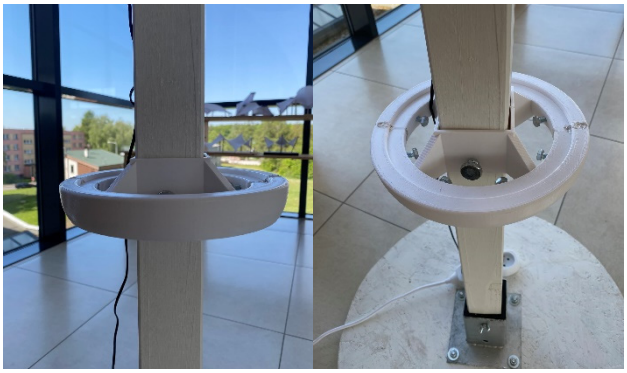

Fig. 2: Prototype of joint of the membrane to the support element made using 3D printing in scale approx. 1:4.

Acknowledgements

This research and this paper were funded by the Ministry of Education, Youth and Sports of the Czech Republic in Student Grant Competition through VSB – Technical University of Ostrava – grant number: SGS SP2024/093.

References

[1] SU, Amanda a Subhi J. AL'AREF. History of 3D Printing. 3D Printing Applications in Cardiovascular Medicine. Online: doi:10.1016/B978-0-12-803917-5.00001-8

[2] CUEVAS, Karla, Mehdi CHOUGAN, Falk MARTIN, Seyed Hamidreza GHAFFAR, Dietmar STEPHAN a Pawel SIKORA. 3D printable lightweight cementitious composites with incorporated waste glass aggregates and expanded microspheres – Rheological, thermal and mechanical properties. Journal of Building Engineering 2021, 44, 102718. ISSN 23527102. Online : doi:10.1016/j.jobe.2021.102718

[4] BUCHANAN, C. a L. GARDNER. Metal 3D printing in construction: A review of methods, research, applications, opportunities and challenges. Engineering Structures. 2019, 180, 332–348 . ISSN 0141-0296. Online: doi:10.1016/J.ENGSTRUCT.2018.11.045

NAVIGATING THE FUTURE OF ADDITIVE CONSTRUCTION: IMPLEMENTING ISO 52939 STANDARDS FOR ENHANCED BUILDING QUALITY

Marcin HOFFMANN[1], Pawel SIKORA[2], Karol FEDEROWICZ[2], Szymon SKIBICKI[2], Mateusz TECHMAN[2], Daniel SIBERA[2], Krzysztof CENDROWSKI[2]

[1]Faculty of Mechanical Engineering and Mechatronics, West Pomeranian University of Technology in Szczecin, Al. Piastów 19, 70-310 Szczecin, Poland

[2]Faculty of Civil and Environmental Engineering, West Pomeranian University of Technology in Szczecin, Al. Piastów 50a, 70-311 Szczecin, Poland

marcin.hoffmann@zut.edu.pl

In the face of increasing demand for construction, as well as difficulties such as labor shortages and negative environmental impacts, the construction sector is increasingly turning towards additive manufacturing technologies (Additive Construction, AC). The ISO/ASTM DIS 52939:2022(E) standard is aimed at regulating this area by providing a framework of qualifications necessary for the production of high-quality additive constructions (Fig. 1.).

The article discusses the scope of the standard, which pertains to construction processes, properties essential for quality, and factors influencing the operation of the AC system. The structure of the production process is presented, from verifying the feasibility of using AC for construction, through project preparation, site preparation, machinery, and shipping. This includes key steps that should be controlled and monitored to ensure the highest quality of printed structures, whether carried out on-site or off-site.

It is noted that this document applies to all additive manufacturing technologies, regardless of the materials used or the process category, for both residential and commercial applications.

This article emphasizes the importance of a standardized approach to the construction process, which allows for risk minimization and provides better durability, sustainability, and cost efficiency compared to traditional construction methods. It also points out the need for further development and harmonization of regulations concerning additive manufacturing technologies in the construction sector, to effectively respond to the dynamically changing needs of the construction market.

The proposed methodologies and approaches presented in ISO 52939 are additionally discussed along with quality measures taken during implementation of “Recycled aggregates for 3D printed concrete structures” (Recycl3D) project.

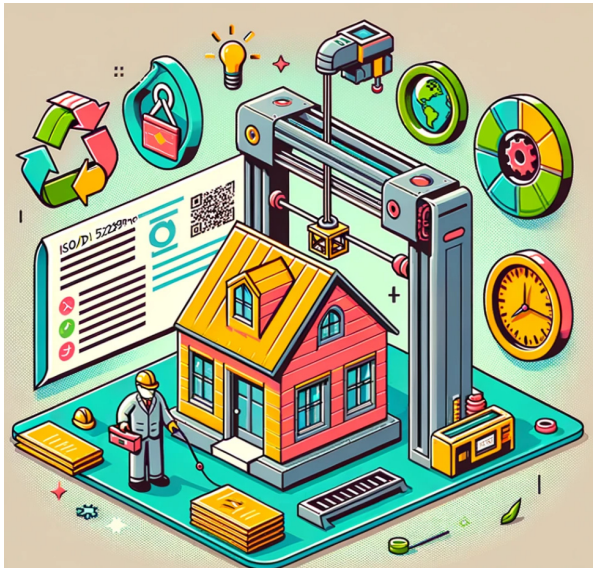

Fig. 1. Graphical concept of ISO 52939 standard for additive construction

Acknowledgements

This research was funded in whole by the National Centre for Research and Development (NCBR), Poland within Project no. ERA-MIN3/140/Recycl3D/2022 (ERA-NET Cofund ERA-MIN3 (Joint Call 2021)).

References

[1] ISO/ASTM 52939:2023 Additive manufacturing for construction, Qualification principles, Structural and infrastructure elements (https://www.iso.org)

FRACTURE-PLASTIC CONSTITUTIVE MATERIAL MODEL OF FRC DEFINED BY THE ATENA PARAMETER IDENTIFICATION SOFTWARE

Marie HORŇÁKOVÁ[1], *Kateřina MATÝSKOVÁ*[2]

[1] Department of Structural Mechanics, Faculty of Civil Engineering, VSB Technical University of Ostrava, Ludvíka Podéště 1875/17, 708 33 Ostrava-Poruba, Czech Republic
[2] Department of Materials, Faculty of Civil Engineering, VSB Technical University of Ostrava, Ludvíka Podéště 1875/17, 708 33 Ostrava-Poruba, Czech Republic

marie.hornakova@vsb.cz, katerina.matyskova@vsb.cz

Fiber-reinforced concrete (FRC) is a material that offers improved toughness, crack resistance, and ductility compared to traditional concrete. Because of these qualities, it is becoming increasingly popular in infrastructure development. However, accurately modeling the fracture-plastic behavior of FRC is challenging due to the complex interaction between the matrix and fibers. To better understand this behavior, advanced computational tools are necessary. This understanding is crucial for designing durable and resilient structures.

This study presents a comprehensive fracture-plastic constitutive material model for structural lightweight waste aggregate concrete (SLWAC). This concrete was made from waste red ceramic fine aggregate, reinforced by copper-coated crimped steel fibers. The experimental data were obtained from a three-point bending test of three specimens with dimensions of 600 mm in length, and 150 mm in height and width. The specimens were notched in the middle, and the load was applied as shown in Fig. 1.

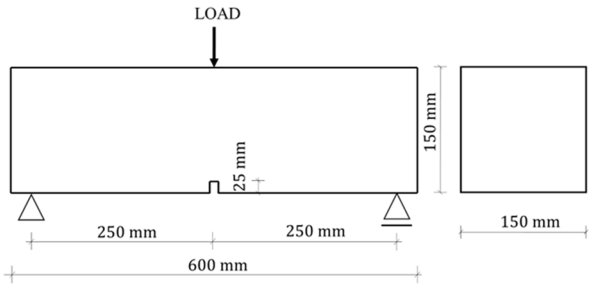

Fig. 1: Model of the 3PBT with the sample dimensions.

For the numerical simulation, GiD v 15.0.1 and ATENA Studio v5 software were used. For the material model, the default *CC3DNonLinCementitious2User* model implemented in ATENA, was utilized. The initial input values for SLWAC with 1.0 % of fibers included a Young's modulus of 8.9 GPa, Poisson's ratio of 0.2, tensile strength of 2.42 MPa, and compressive strength of 12.50 MPa. The first simulation was conducted using these parameters. Then, the ATENA parameter identification software (APIS) was used to determine the tensile function for improved numerical simulation with a targeted similarity error of the two curves of 5 %.

Subsequently, APIS was used to adjust the tensile function (see Fig. 2) based on the average *l-d* diagram obtained from three experiments. In order to align the peaks in the graphs, the Young's modulus needed to be modified to 2.0 GPa. After 4 iterations, APIS successfully achieved a similar diagram (see Fig. 3), with the error determined by APIS as 4.5%.

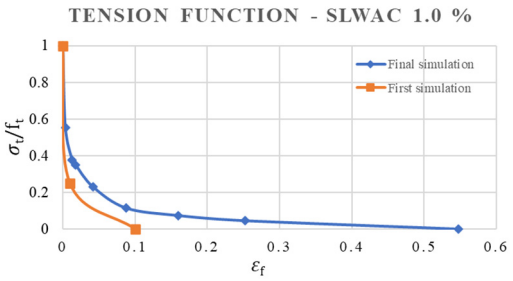

Fig. 2: Tensile function of SLWAC 1.0 %

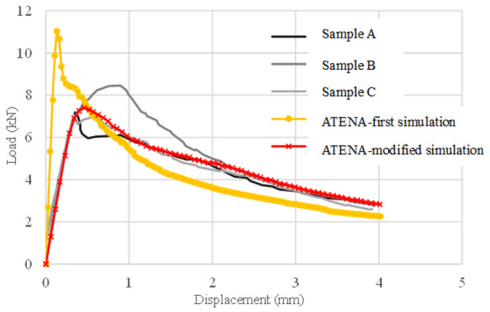

Fig. 3: Load-displacement diagram for SLWAC 1.0 %

Acknowledgements

The research was funded by the Ministry of Education, Youth and Sports of the Czech Republic through VSB – Technical University of Ostrava (SGS SP2024/097).

NUMERICAL AND EXPERIMENTAL ANALYSIS OF THE LOAD-CARRYING CAPACITY OF A TIMBER SEMI-RIGID CONNECTION

Marek JOHANIDES[1], *Antonín LOKAJ*[1]

[1] Department of Structures, Faculty of Civil Engineering, VSB – Technical University of Ostrava, 708 00 Ostrava - Poruba, Czech Republic

marek.johanides@vsb.cz, antonin.lokaj@vsb.cz

Abstract. *The paper describes the load-carrying capacity of a timber semi-rigid connection. The load-carrying capacity was calculated on the basis of the currently valid standard, experimental test and numerical model. The connection was made from the standard combination of bolts and dowels.*

1. Introduction

Despite today's knowledge, the joints of timber structures are still not fully researched. The article describes a comparison of carrying capacity of the timber semi-rigid connection. The results of the experimental testing were compared with the numerical model and values that can be calculated according to the standard for designing timber structures EC5.

The table 1 shows the values where, $F_{,max}$ is the load carrying capacity. Value is in the first three lines obtained by experimental testing, in the fourth line is the value obtained by the numerical model and in the last one is the value calculated as the characteristic bearing capacity according to the EC5 standard (ULS,k and ULS). *U* is the measured deformation during testing, or it is a value from a numerical model. *M* is the recalculated bending capacity of the connections.

Fig. 1 shows a scheme of a solved connection, fig. 2 shows the load-deformation curve of individual experimental tests and numerical modeling and in tab.1 individual results are shown and compared.

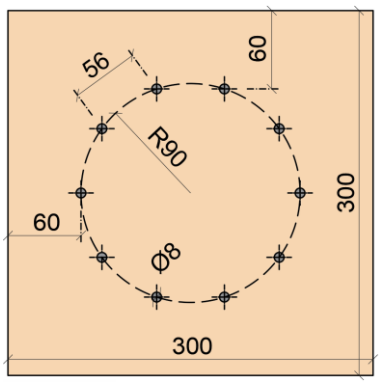

Fig. 1 Connection detail.

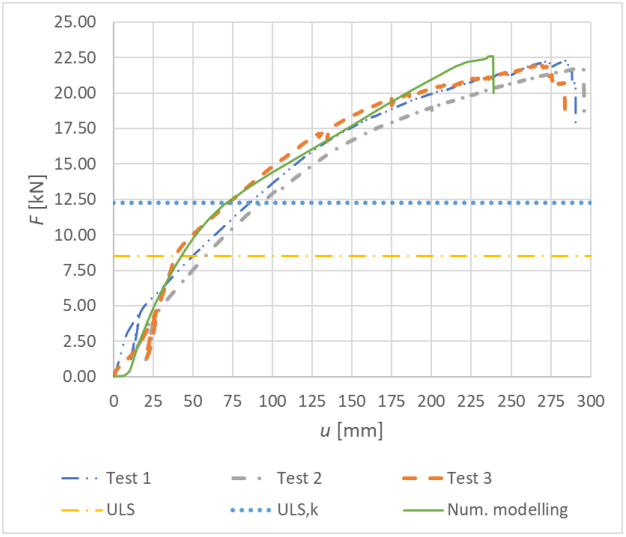

Fig. 2 Load–deformation curves for Bolts and dowels.

Tab. 1 Results of Load Carrying capacity.

Specimen	$F_{,max}$ [kN]	*u* [mm]	*M* [kNm]
Exp. 1	22.29	290.50	19.03
Exp. 2	21.78	271.85	18.76
Exp. 3	22.02	247.10	18.98
Num. model	22.60	238.64	17.40
EC5,k (ULS,k)	12.26	-	15.94
EC5,d (ULS)	8.51	-	11.06

2. Conclusion

The paper presents and compares the results obtained by experimental testing, numerical modelling and the results calculated according to the EC5 standard. In the results, it is possible to observe a fairly good agreement achieved between experimental testing and numerical modeling. Also, the safety of this connection was proven based on the difference of the residual load capacity between the EC5 calculation and the experimental test.

SHEAR STRENGTH OF 3D PRINTED FFF/FDM SAMPLES

David JURAČKA[1], *Petr LEHNER*[1], *David BUJDOŠ*[2] , *Martin KREJSA*[1]

[1] Department of Structural Mechanics, Faculty of Civil Engineering, VSB-Technical University of Ostrava, Ludvika Podeste 1875/17, 708 00 Ostrava-Poruba, Czech Republic
[2] Department of Building Materials and Diagnostics of Structures, Faculty of Civil Engineering, VSB – Technical University of Ostrava, Czech Republic

david.juracka@vsb.cz, petr.lehner@vsb.cz, david.bujdos@vsb.cz, martin.krejsa@vsb.cz

3D printing opens the door to previously unattainable design possibilities, especially through the creation of special details that would otherwise be difficult or impossible to produce with traditional methods.

An element made using additive manufacturing technology called FFF/FDM (Fused Filament Fabrication/Fused Deposition Modeling) has an orthotropic character if the printed filaments are arranged in one direction. Therefore, they have different mechanical properties in different directions. Currently, there is no standard examining shear properties, and therefore it is necessary to create your own laboratory test with original designed sample. For these purposes, the tensile test and the sample with the weakest point at the point of contact of the fibers, where the smallest load-bearing capacity can be assumed, were chosen (see Fig.1). A printed fiber with a size of 0.2 by 0.4 mm was chosen for these samples.

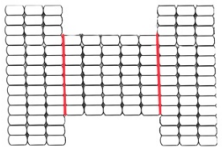

Fig. 1: Schematic cross-section showing the individual fibers in the stressed point of the sample with a prominent position of the assumed failure in shear.

Ansys Workbech/Mechanical software was used for the detailed model and subjected to a tensile test. The model is made up of 3D printed PC Blend (polycarbonate). For numerical calculations the sample was simplified without distinguishing individual fibers. The result is a von Mises equivalent stress (see Fig.2).

In the model, the following material properties are set for the 3D printed element: modulus of elasticity in tension is 1.9 GPa, tensile strength is 63 MPa, Poisson's constant is 0.4 and density is 1220 kg/m^3. According to this design, a sample was printed and tested in the laboratory. The assumption is the stress distribution and its maximum value in the places where the layers of the weakest part are connected. Its resulting working graph is shown in Figure 3. The maximum tensile load force (F) achieved was 3.9 kN with a displacement of 5.6 mm when the specimen completely failed. However, the failure occurred partially at the junction between the fibers and elsewhere these fibers were overstressed, which may indicate that the shear capacity is almost similar to the tensile capacity.

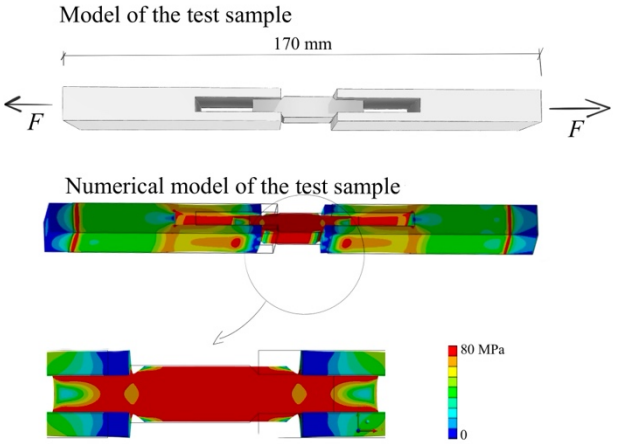

Fig. 2: Schematic of the specimen with the stress direction marked and comparison with the numerical model from Ansys software with von Mises equivalent stress design

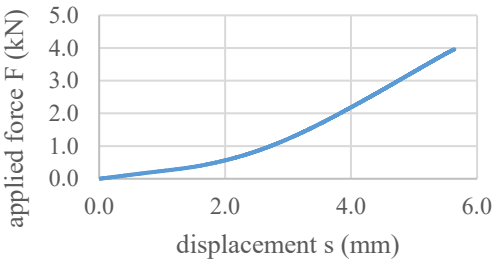

Fig. 3: Load-displacement diagram of specimen tested in tension

Acknowledgements

This research and this paper were funded by the Ministry of Education, Youth and Sports of the Czech Republic in Student Grant Competition through VSB – Technical University of Ostrava – grant number: SGS SP2024/093.

ASSESSMENT OF THE CONDITION OF THE A6 MOTORWAY PAVEMENT WITH RECYCLED AGGREGATE ROAD BASE

Robert JURCZAK[1]

[1] Department of Construction and Road Engineering, Faculty of Civil and Environmental Engineering, West Pomeranian University of Technology in Szczecin, Al. Piastów 50a, Szczecin, Poland

Robert.Jurczak@zut.edu.pl

The concrete pavement of the A6 motorway required replacement after 68 years of use due to its poor condition. There was damage typical of this type of pavement, i.e. corner cracks and transverse cracks in the slabs. In addition, the existence of transverse thresholds and faults in the pavement was felt while driving. Therefore, at the end of 2005 its reconstruction began and included both carriageways on the section from km 13+937 to km 21+672 (Klucz-Kijewo). The main aim of the reconstruction was to improve road safety and driving comfort. The new 7.74 km section of the motorway was opened to traffic in September 2007. As part of this task, 12 viaducts, a bridge and a flyover were also rebuilt.

The reconstruction consisted of demolishing the old concrete pavement, widening it and making a completely new asphalt pavement with using demolition material. A scheme and layout of the individual layers of the designed pavement construction are shown in Fig. 1.

The composition of the asphalt concretes (AC) and stone mastic asphalt (SMA) was typical of this type of material used on national roads in the West Pomeranian Voivodship. The non-typical material used for the new pavement structure was concrete rubble obtained by crushing pre-broken pavement slabs in a crusher at the building area.

A detailed characterization of concrete (including petrographic analysis) and concrete rubble recovered from the pavement of the A6 motorway in use for several decades is presented in the article [1].

An analysis of the photographic documentation carried out during the last field inspection shows that the asphalt pavement with a sub-base of concrete aggregate obtained from crushed slabs after 17 years of service is in good technical condition. No deformations have been observed. The pavement is even, without any collapses. The only significant damage to the pavement is transverse cracks (Fig. 2). During the inspection, 44 transverse cracks were found (25 on the north carriageway and 19 on the south carriageway).

On the basis of the assessment of the technical condition of the A6 motorway after 17 years of service, the full suitability of recycled concrete pavement materials for their reuse in new pavement layers can be confirmed. Moreover, they can be an alternative source of aggregates, replacing natural aggregates. In the author's opinion, the positive experience so far obtained under real conditions shows the great potential of this type of (semi-rigid) pavement in carrying significant traffic loads.

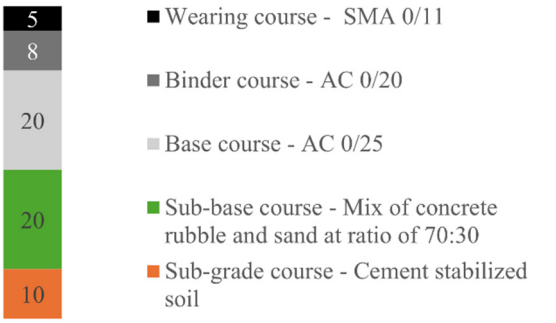

Fig. 1: Graph. describing a development of the variable z (unit) depending on the value of x (unit) and y (unit).

Fig. 2: View of an example of a transverse crack in the A6 motorway pavement after 17 years of service

References

[1] Rudnicki, T.; Jurczak, R. Recycling of a Concrete Pavement after over 80 Years in Service. Materials 2020,13, 2262. https://doi.org/10.3390/ma13102262.

OBTAINING THE COORDINATES OF THE POSITION OF THE SPHERE FROM VIDEO FOOTAGE

Marek KAWULOK[1,2], *Stanislav POSPÍŠIL*[1,2], *David JURAČKA*[1]

[1]Department of Structural Mechanics, Faculty of Civil Engineering, VSB – Technical University of Ostrava, Ludvika Podeste 1875/17, 708 00 Ostrava-Poruba, Czech Republic
[2]Institute of Theoretical and Applied Mechanics of the Czech Academy of Sciences, Prosecka 809/76, 190 00 Prague 9, Czech Republic

marek.kawulok@vsb.cz, stanislav.pospisil@vsb.cz, david.juracka@vsb.cz

The ball vibration absorber is a representative of passive damping devices. Such a damper consists of a supporting bowl and an inner ball. This absorber has several advantages, including its relatively small size, wide range of possible frequency tuning, and minimal maintenance requirements. On the other hand, there are some complications arising from the non-linear nature of the system. These are mainly associated with motion instabilities, bifurcations, and autoparametric oscillations. Numerical investigation of the dynamic response of the ball absorbers also shows that the non-linear nature of the system is a factor, which makes the resonance curves strongly dependent on the excitation amplitude. With increasing excitation force amplitude, a stronger softening effect of the resonance curves was observed. Numerical simulations are able to provide valuable information about the behaviour of a dynamic system described by equations of motion. However, during their derivation, simplifications are implemented in order to improve the analytical relations. Therefore, it is desirable to validate the obtained results experimentally.

However, in the case of experimental measurements of the response of this type of absorber, the question is how to obtain information about the motion of the sphere. The aim of this contribution is to present an algorithm that can detect and track the position of a sphere based on the analysis of video recordings of experimental measurements. Using MATLAB software, the analysis is performed in several main steps. In the first step, the sphere object is separated from the background, which can cause difficulties in subsequent sphere detection. Detection is performed by applying the Circle Hough transform [1]. This transform can determine the contour and centre of the sphere in each frame of the video based on the pre-defined radius of the sphere. This approach can detect the sphere even if only part of it is visible. Applying this algorithm to all frames of the video, it is possible to obtain information about the position and behaviour of the sphere over time. So far, the algorithm has only been used to analyse the free vibration response of the sphere. An example of the original video frame and the same frame after applying the algorithm can be seen in Fig.1.

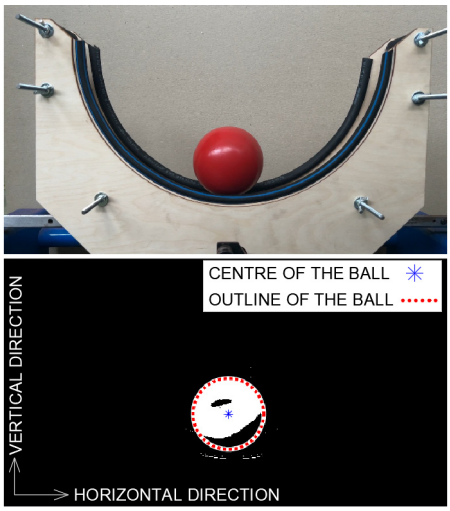

Fig. 1: Example of the raw frame (upper) and the same frame after the application of the algorithm (lower).

Acknowledgements

The financial support of the grant program financed by the Ministry of Education, Youth and Sports of the Czech Republic through VSB–TUO SGS SP2024/069 and from the budget for conceptual development of science, research and innovations is highly acknowledged.

References

[1] FLORES-MENDEZ, Alejandro and SUAREZ-CERVANTES, Angeles, 2009. Circular Degree Hough Transform. Online. In: BAYRO-CORROCHANO, Eduardo and EKLUNDH, Jan-Olof (eds.). Progress in Pattern Recognition, Image Analysis, Computer Vision, and Applications. Lecture Notes in Computer Science. Berlin, Heidelberg: Springer Berlin Heidelberg, p. 287-294. Available at: https://doi.org/10.1007/978-3-642-10268-4_34.

Numerical Study of the Effect of Maturation and Extended Chloride Deposition on Chloride Ingress

Petr KONEČNÝ[1], *Petr LEHNER*[1], *Marie HORŇÁKOVÁ*[1]

[1] Department of Structural Mechanics, Faculty of Civil Engineering, VSB – Technical University of Ostrava, L. Podéště 1875, Ostrava, Czech Republic

petr.konecny@vsb.cz, petr.lehner@vsb.cz, marie.hornakova@vsb.cz

The durability of steel reinforced concrete in chloride ladden environment requires description of the penetration of chlorides to the level of steel reinforcement in order to evaluated the risk of corrosion. Such analysis is important task that involve both experimental evaluation as well as numerical modeling. Typical analytical models for the evaluation of concentration do not account for the delay of the exposure to chlorides. However, model capturing even delayed exposure to chlorides are discussed in [2]. There are also finite element based models for chloride ingress with delayed chloride penetration that can handle the delayed exposure, e.g. [1].

The aim of this contribution is to compare analytical and numerical models suitable to simulate the chloride ion penetration in the concrete with delayed chloride ingress. Such comparison is a preparation for subsequent comparison of the modeled values with measured data that will be result of experimental campaign. Diffusion coefficient and aging factors will be based on the measurement from chloride profile obtained in laboratory conditions. The description of chloride ingress will be based on analytical formula proposed by [3] and criticized in [2]:

$$\frac{C}{C_s} = 1 - erf\left(\frac{x}{2\sqrt{D_0 \cdot \left(\frac{t'_0}{t+t'_{ex}}\right)^n \cdot t}}\right) \qquad (1)$$

where C is the chloride concentration, C_s is the surface chloride concentration, x is the investigated depth, D_0 is the reference diffusion coefficient, n is aging factor, t'_0 is reference concrete age, t is exposure period and t'_{ex} is the concrete age when the exposure starts. Since Luping in [2] challenges the diffusion coefficient D_0, the modification of D_0 given in Eq. (2):

$$D_a = D_0 \cdot \frac{f(t'_{ex})}{1-n} \cdot \left(\frac{t'_0}{t}\right)^n, \qquad (2)$$

where $f(t'_{ex})$ is function given in Eq. (3), will be evaluated as well.

$$f(t'_{ex}) = \left[\left(1 + \frac{t'_{ex}}{t}\right)^{1-n} - \left(\frac{t'_{ex}}{t}\right)^{1-n}\right]. \qquad (3)$$

Results from Eq. (1) and its modification with Eq. (3) will be compared with the results from transient finite element model used in [1].

Acknowledgements

This contribution has been developed as a part of the research project GACR 22-19812S "Effect of gaseous and traffic induced pollutants on the durability of selected construction materials" supported by the Czech Science Foundation.

References

[1] KONEČNÝ, P., LEHNER, P., PUSTKA, D. Reinforced Concrete Bridge Deck Model Considering Delayed Exposure to Chlorides. Periodica Polytechnica Civil Engineering. 2019. ISSN: 1587-3773 Available from: doi.org/10.3311/PPci.13780

[2] LUPING, T. and GULIKERS, J. On the mathematics of time-dependent apparent chloride diffusion coefficient in concrete. Cement and Concrete Research. 2007. ISSN: 1873-3948. Available from: doi.org/10.1016/j.cemconres.2007.01.006

[3] M. MAAGE, M., HELLAND, S., CARLSEN, J.S. Practical non-steady state chloride transport as a part of a model for predicting the initiation period, in: NILSSON,L.O., OLLIVIER, J. (Eds.), Chloride Penetration into Concrete, RILEM PRO, vol. 2, 1995, pp. 398–406.

COMPLEX MATERIAL CHARACTERISTICS OF CFRP LAMINATE COMPOSITE WITH DEFECT

Eva KORMANIKOVA[1], *Kamila KOTRASOVA*[1]

[1]Institute of Structural Engineering, Technical University of Košice, Vysokoškolská 4, 042 00 Košice, Slovakia

eva.kormanikova@tuke.sk, kamila.kotrasova@tuke.sk

The determination of the mechanical properties is essential for ensuring performance in designing composite structures. In addition, the knowledge of the complete elastic stiffness matrix is important for modelling and evaluating the mechanical behaviour of composite materials under several loading conditions [1].

The current test methods for measuring engineering constants are not well established. Although typically a tensile test or three-point bending test is being used, the relevant standards are mainly focusing in measuring the full stress-strain curve. The elastic part is only a small item in this curve. The ASTM E111 [2] standard is focussing on the issues relevant to have an accurate Young's modulus, Tangent modulus, and Chord modulus measurement. Alternatively dynamic methods like the Impulse Excitation Technique (IET) are used to measure the complex engineering constants. They have the advantage that they are quite fast, simple and non-destructive.

The set of UD carbon fiber reinforced samples with built in defects in half of the surface of the samples consists of UD beam 1, 90° beam 2 and a Poisson plate (Fig. 1). The first resonance frequency of the test beams and the three first resonance frequencies of the test plate are measured with a small accelerometer. These frequencies are compared with the computed frequencies using accurate FE models of the test specimens. The in-plane orthotropic engineering constants (E_1, E_2, ν_{12} and G_{12}) are iteratively tuned in the FE models in such a way the computed frequencies match the measured frequencies.

The goal of the investigation is to verify if the defects affect the complex engineering constants. The real parts of the engineering constants are only affected a little bit by the defects. The damping parts (tangents delta) are more affected. Especially the tangents of Poisson ratio changes considerably. The physical background of the tangents delta of the engineering constants E_1, E_2 and G_{12} is that they are phase shifts between stresses and strains during sinusoidal vibrations in stationary regime. The value of these phase shifts is always positive. The physical background of the tangent delta of Poisson's ratio is more complex and has never been thoroughly investigated in scientific papers. It is a phase shifts between two sinusoidal strains in both orthotropic directions. The value of the tangents delta seems to adapt itself to make the complex stiffness matrix symmetric. The value can be positive as well as negative (Table 1).

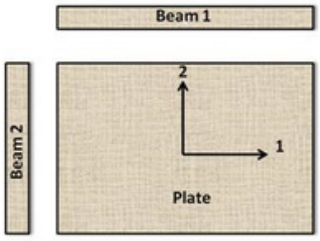

Fig. 1: UD beam (Beam 1), a 90° beam (Beam 2) and a Poisson plate (Plate).

Engineering constants	Purely UD carbon	UD carbon with defects
Elastic part E1	1.023E11 Pa	1.051E11 Pa
Elastic part E2	7.495E09 Pa	8.042E09 Pa
Elastic part v12	0.386	0.419
Elastic part G12	3.671E09 Pa	4.034E09 Pa
Tangent E1	0.068 %	0.136 %
Tangent E2	0.640 %	0.640 %
Tangent v12	2.332 %	-1.917 %
Tangent G12	1.650 %	1.009 %

Tab.1: Comparison of results with and without defects

Acknowledgements

We thank the projects VEGA1/0363/21, and 1/0307/23 for financially supporting this work. We would like to thank the BYTEC BV, Belgium for realization of Resonalyser tests.

References

[1] V. M. Cuartas, M. Perrin, M.L. Pastor, H. Welemane, A. Cantarel, et al. Determination of the elastic properties in CFRP composites: comparison of different approaches based on tensile tests and ultrasonic characterization. Advances in Aircraft and Spacecraft Science, Techno-Press, 2(3), 249-260, 2014.

[2] ASTM-E111: Standard Test Method for Young's Modulus, Tangent Modulus, and Chord Modulus, 2017.

THE INFLUENCE OF THE REINFORCEMENT LAYER ORIENTATION ON THE RESPONSE OF MULTILAYERED COMPOSITE PLATES

Kamila KOTRASOVA[1], *Eva KORMANIKOVA*[2]

[1] Department of Structural Mechanics, Institute of Structural Engineering and Transportation Structures, Faculty of Civil Engineering, Technical University of Košice, Vysokoškolská 4, 042 00 Košice, Slovakia

kamila.kotrasova@tuke.sk, eva.kormanikova@tuke.sk

The use of the laminated composites in many engineering applications has expanded rapidly over the past four decades. In particular, laminated composite plates are often used in various engineering applications and have widespread economic use in various fields of science, including aerospace, marine, mechanical, and modern highways. The use of composite plates in construction, bridges, can lead to economic solutions and allows the construction of straight, aesthetic, and safe highways necessary to increase the speed of current traffic.

The required knowledge, which is necessary to know how to manage composite materials, composite structural elements, requires FEM numerical simulations.

The simply supported square laminate plate L x L: 20 cm x 20 cm with the thickness h = 1 cm is considered. The uniform transverse pressure load q = 1 MPa is subjected on laminate plate. The lay-up is made of three layers, all with the same thickness. Each layer has the same orthotropic material properties:
$E_a = 30 \cdot 10^4$ MPa, $E_b = 1 \cdot 10^4$ MPa, $E_c = 1 \cdot 10^4$ MPa,
$G_{ab} = 1 \cdot 10^4$ MPa, $G_{ac} = 0.5 \cdot 10^4$ MPa, $G_{bc} = 0.5 \cdot 10^4$ MPa,
$\nu_{ab} = 0.01$, $\nu_{ac} = 0.01$, $\nu_{bc} = 0.3$.
The material axes are different in each layer. The layers 1, 2 and 3 are oriented at 0, 45 and 90 degrees from the axe x.

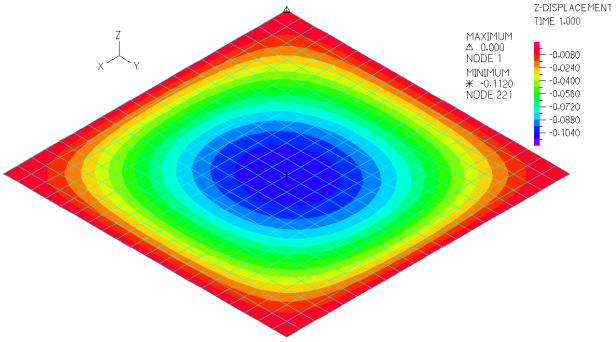

Fig. 1: The vertical displacement of the square laminate plate with ply orientation 0/90/0.

The vertical displacement at the centre of the square laminate plate with ply orientation 0/90/0 is documented in Fig. 1. Fig. 2 shows the diagram of vertical displacement of the square laminate plate with ply orientation 0/90/0 at the centre lines in direction of axis x and y, respectively. Blue line shows the vertical displacement diagram of the square laminate plate with ply orientation 0/90/0 at the centre lines in direction x and red line in direction y.

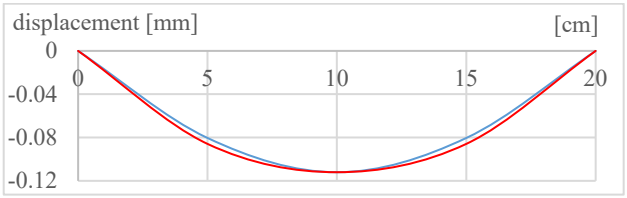

Fig. 2: The vertical displacement at the centre perpendicular lines of the square laminate plate with ply orientation 0/90/0.

Fig. 3 presents the comparison of the vertical displacements at the centre of the square laminate plate with next considered ply orientations as 0/45/90, 45/-45/45 and 0/90/0.

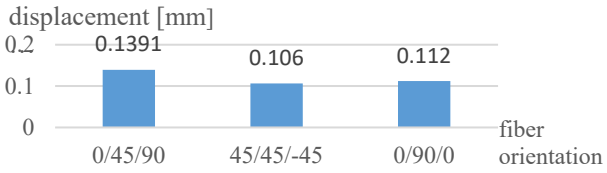

Fig. 3: Comparing of the vertical displacements at the centre of the square laminate plate with ply orientations 0/45/90, 45/-45/45 and 0/90/0.

Acknowledgements

We thank the Scientific Grant Agency VEGA 1/0307/23 and 1/0642/24.

References

[1] Pagano, N.J., "Exact solutions for rectangular bidirectional composites and sandwich plates", J. Comp. Mat., 4, pp. 20-34, 1970.

NUMERICAL SOLUTION OF NATURAL FREQUENCIES AND MODE SHAPES

Lenka KOUBOVA[1]

[1]Department of Structural Mechanics, Faculty of Civil Engineering, VSB-Technical University of Ostrava, Ludvika Podeste 1875/17, 708 00 Ostrava-Poruba, Czech Republic

lenka.koubova@vsb.cz

Every construction has a set of their natural frequencies (resonant frequencies) and mode shapes that depends on its material, structure and boundary conditions. A mode shape is a deflection pattern. It is related to a particular natural frequency and represents the relative displacement $u_{(t)}$ of all parts of a construction for that particular mode.

The method of stiffness constants is method used to determine natural frequencies and mode shapes in this case. The solved construction is replaced by computational model, i.e. with system with n degrees of freedom. A mass matrix [**m**] and a stiffness matrix [**k**] is derived. The equations of motion can be written (in matrix notation):

$$[\mathbf{m}]\{\ddot{\mathbf{u}}_{(t)}\} + [\mathbf{k}]\{\mathbf{u}_{(t)}\} = \{0\}. \quad (1)$$

It is assumed that the construction vibrates in the harmonic motion. Then equations of motion can be rewritten into the equation:

$$\left[[\mathbf{k}] - \omega_n^2 \cdot [\mathbf{m}]\right]\{\mathbf{u}_{(t)}\} = \{0\}. \quad (2)$$

We are looking for the zero determinant of the matrix $\left[[\mathbf{k}] - \omega_n^2 \cdot [\mathbf{m}]\right]$, this gives us the natural frequencies ω_n. The determining of zero determinant is numerical in this solution. The values of natural frequency are chosen with the given difference and the determinant is calculated. In the section where the sign of the determinant changes, the value of the natural frequency is found (see Fig. 1). Bisection method is used.

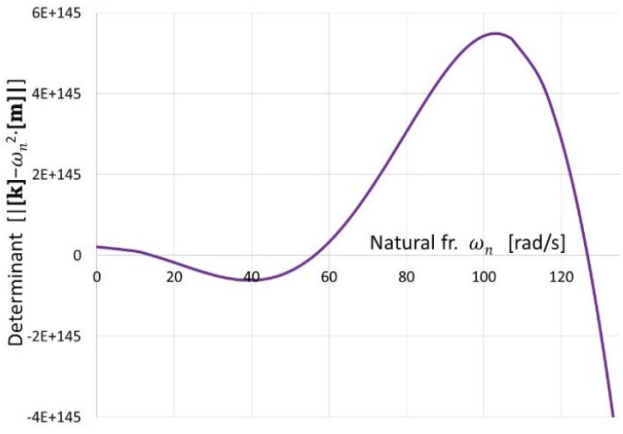

Fig. 1: Numerical solution of natural frequency of simple beam using the zero determinant of a matrix.

The procedure was first applied to a simple beam for which the first natural frequency can be determined as $\omega_n = \sqrt{k/m}$. The mass m is taken as half the mass of the beam. The stiffness k of the simple beam is $k = 48 \cdot EI/l^3$. First natural frequency is ω_n = 13.975 rad/s for concrete beam with l = 16 m, h = 0.4 m, b = 1 m. Natural frequency ω_1 = 14.078 rad/s was solved numerically using the given procedure. The difference between the values is 0.7%.

This procedure can be used for any construction with mass matrix [**m**] and stiffness matrix [**k**]. It was also used to solve the parabolic arc. The arc was divided into 16 elements. Computational model with 47 degrees of freedom was created. Fig. 2 shows the 3rd and 6th mode shape of the solved arc. The 3rd mode shape of arc was set for natural frequency ω_3 = 95.699 rad/s and 6th mode shape was set for natural frequency ω_6 = 759.668 rad/s.

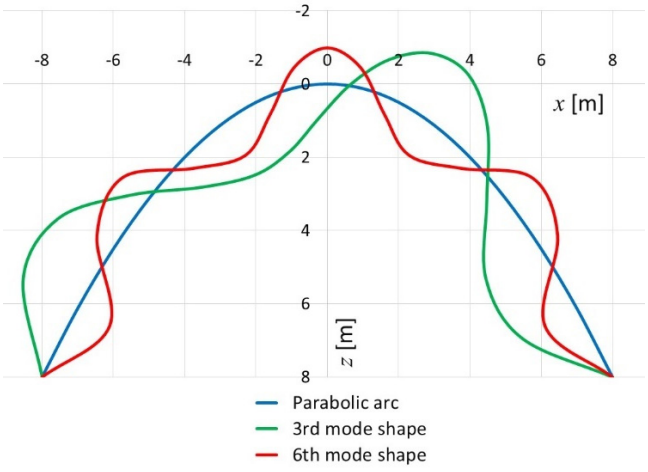

Fig. 2: The 3rd and 6th mode shape of the parabolic arc.

Acknowledgements

Financial support from VSB-Technical University of Ostrava by means of the Czech Ministry of Education, Youth and Sports through the Institutional support for conceptual development of science, research and innovations is gratefully acknowledged.

CRITICAL DISTANCE OF HDPE AND ITS USE IN FATIGUE LIFETIME PREDICTIONS

Kamila KOZÁKOVÁ[1,2], *Lukáš TRÁVNÍČEK*[3], *Jan KLUSÁK*[1], *Jan PODUŠKA*[1], *Pavel HUTAŘ*[1]

[1] Institute of Physics of Materials, Czech Academy of Sciences, Žižkova 513/22, 616 00 Brno, Czech Republic
[2] Faculty of Mechanical Engineering, Brno University of Technology, Technická 289/2, 616 69 Brno, Czech Republic
[3] Materials Science and Testing of Polymers, Montanuniversität Leoben, Otto Glöckel-Strasse 2, 8700 Leoben, Austria

kozakova@ipm.cz, lukas.travnicek@unileoben.ac.at

Geometrical discontinuities (holes, fillets, and grooves) are unavoidable in the design of components. When these components are loaded, the geometrical discontinuities act as stress concentrators. Notches require special attention, especially in fatigue, as their presence reduces the resistance of a component to failure.

The contribution analyses the fatigue lifetime of cracked round bar (CRB) specimens and the specimens with V-notches (the notch radii: 0.1, 0.2, and 0.4 mm) made of HDPE. Fatigue lifetime predictions of notched specimens are performed using critical distances [1]. The fatigue tests are performed at the INSTRON E3000 with a sinusoidal loading at a frequency of 10 Hz.

The objective of the study can be achieved by the following two steps: determination of the critical distance l_{cr} based on fatigue data measured on CRB specimens and on one of the notched specimens, and the prediction of fatigue lifetime of the other two notches.

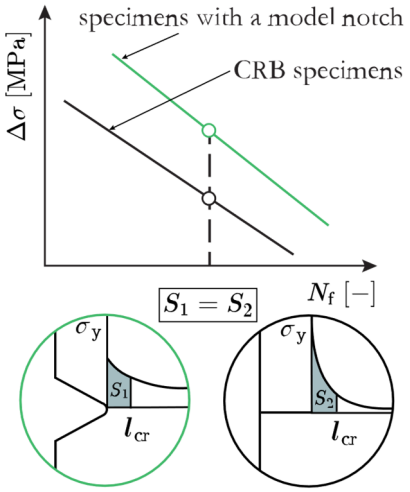

Fig. 1: Determination of the critical distance l_{cr}

The critical distance is determined from the equality of the average stresses over l_{cr} for a CRB specimen and a specimen with a model notch, as shown in Fig. 1. The comparison is done for the same number of cycles to failure of both cases. This process of l_{cr} determination is repeated for the whole range of number of cycles to failure N_f. The critical distance depends on N_f, but also on the notch radius. For this reason, the critical distance l_{cr} is modified by the ratio of stress concentration factors: $l_p = l_{cr}.K_{tp}/K_{tm}$, where l_p is the critical distance used for fatigue lifetime determinations of the predicted notch, K_{tp} and K_{tm} are the stress concentration factors of the predicted notch and model notch, respectively.

Fig. 2 shows the fatigue lifetime predictions of notches with $r = 0.1$ and 0.4 mm based on l_{cr} determined from CRB specimens and notched specimens with $r = 0.2$ mm.

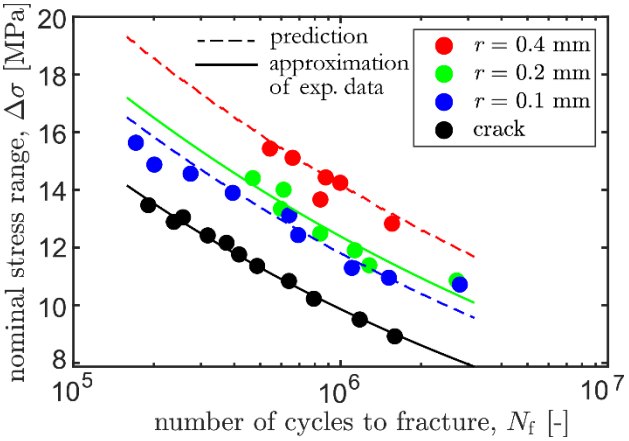

Fig. 2: Fatigue lifetime predictions of notched specimens (HDPE)

Acknowledgements

The work was supported by the projects of BUT (FSI-S-23–8240) and Czech Science Foundation (21-14886S).

References

[1] TAYLOR, David. The theory of critical distances. Engineering Fracture Mechanics, 2008, 75.7: 1696-1705.

NUMERICAL MODEL OF 3D PRINTED JOINT OF WOODEN FRAME

Petr LEHNER[1], *David JURAČKA*[1], *Dominik GŘEŠICA*[1], *Martin KREJSA*[1]

[1] Department of Structural Mechanics, Faculty of Civil Engineering, VSB-Technical University of Ostrava, Ludvika Podeste 1875/17, 708 00 Ostrava-Poruba, Czech Republic

david.juracka@vsb.cz, petr.lehner@vsb.cz, dominik.gresica.st@vsb.cz, martin.krejsa@vsb.cz

Regardless of the type of material, 3D printing seems to be an interesting alternative to conventional construction methods. Leaving aside the use of 3D printing systems for concrete or cement composites, the more conventional 3D printing of plastic, metal or other separated materials may also have its hypothetical benefits in the creation of structural joints. For truss structures, such as arch bridges, certain types of joints can be expected that do not always have the same angle between the single-plane load-bearing elements of the structure. In such a case, the use of 3D printing technology for joint fabrication is defensible. In the case of a standard scale and using experience from timber bridges, one would assume that an embedded plate and pin connection would be the appropriate connection form. In contrast, from the point of view of producing smaller physical models, mainly for a deeper understanding of the comparability issues of numerical modelling and experimental testing, it is advantageous to use so-called enveloping timber element connections.

The present paper describes the basic process of designing, numerical analysis and evaluation of a global structural model of a wooden arch bridge with emphasis on modelling the connection detail using 3D printed polycarbonate joints. Fig. 1 shows a simplified numerical model prepared in Scia Engineering to obtain the basic boundary conditions for the numerical model of the coupling. C24 wood is used as the primary material and the cross-sections of the elements are 10 x 10 mm. The spacing of the bridge supports is 1000 mm.

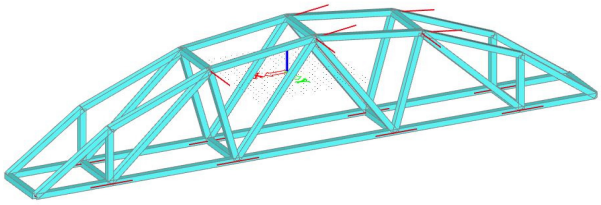

Fig. 1: Global numerical model.

Ansys Workbech/Mechanical software was used for the detailed model. The model is made up of parts of wooden members and mainly a precisely prepared 3D printed joint. This model has clearly defined boundary conditions to infer the thrust in the diagonal direction. The contacts between the materials are set to a friction value of 0.4 and the model also contains 2 joints simulating a bolt (See Fig.2). Contacts between materials only allow the transfer of compressive forces.

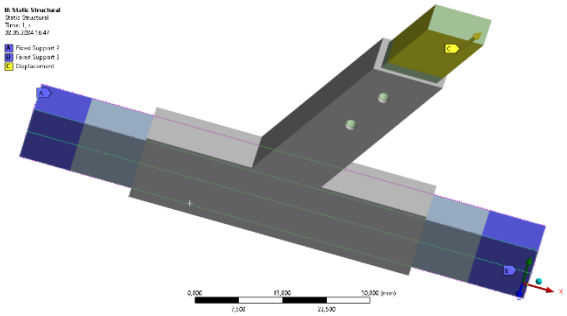

Fig. 2: Boundary conditions of the numerical model of join.

In the model, the following material properties are set for the 3D printed element: modulus of elasticity in tension is 1.9 GPa, tensile strength is 63 MPa, Poisson's constant is 0.4 and density is 1220 kg/m^3. 3D printed structures have problems with delamination of individual layers and this effect should be further investigated in the numerical model. The present paper shows a first step in this direction, introducing a finite element mesh of the size of each printed layer in the model. An example of the deformation in a section plan joint is shown in Figure 3.

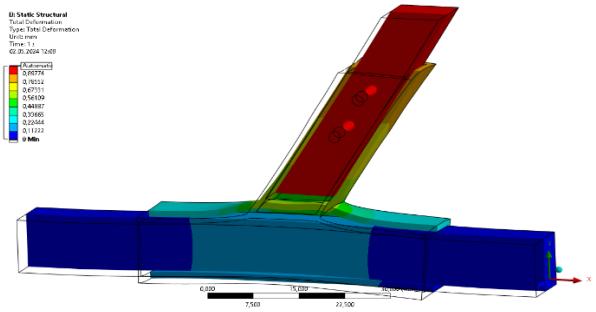

Fig. 3: Example of deformation results.

Acknowledgements

This research and this paper were funded by the Ministry of Education, Youth and Sports of the Czech Republic in Student Grant Competition through VSB – Technical University of Ostrava – grant number: SGS SP2024/093.

ELASTIC MODULUS DETERMINATION IN LOW-STRENGTH CEMENT-BOUND MIXES

Stanisław MAJER[1], *Bartosz BUDZIŃSKI*[1]

[1] Department of Construction and Road Engineering, Faculty of Civil and Environmental Engineering, West Pomeranian University of Technology in Szczecin, Piastów Street 50a, Szczecin, Poland

stanislaw.majer@zut.edu.pl, bartosz.budzinski@zut.edu.pl

Elastic modulus (E) is one of the parameters defining elastic behaviour of a material under analysis. It represents the resistance of a given material to elongation or contraction in the elastic or Hooke's law region of its behaviour. Elastic modulus or Young's modulus is highly relevant to structural design by influencing, together with the thickness of components, the structural rigidity of the system.

In the case of cement-bound materials its value depends on the content of cement in the mix, and thus their compressive strength. Concrete is not an isotropic material having tensile strength in the range of 6-9% of its compressive strength. With decreasing strength the linear expansion coefficient also decreases. This property is used to characterise bottom layers of road pavements, which are considered flexible when their compressive strength is lower than 5 MPa.

Flexibility of cement-bound mixes was a very important characteristic for cryogenic tanks design, prepared as part of the LNG terminal construction project, located in Świnoujście, Poland. The applied technology yields ca. 600 m^3 of gas supplied to end users from 1 m^3 of LNG cooled to –163°C at atmospheric pressure. The decision to proceed with the project, whose strategic importance for Poland and its neighbours must not be underestimated, was taken in 2006 and in 2015 terminal was put in service, which is considered a very short time span. Two cryogenic tanks of 160,000 m^3 capacity each were design, including allowance for future expansion with a third tank. The third tank will be put in service in the third quarter of 2024. From geological point of view, the terminal is located within the Brama Świny formation, which is the terminal part of the Lower Odra river valley. Brama Świny was formed by a few dozen spits, partly transformed by aeolical processes. The formation was built in the Holocene, when raising sea levels resulted in several marine transgressions. When the sea has receded, sedimentation started in the glacial river valleys and depressions, forming spits of the current Wolin and Uznam islands and partly cutting off the Odra Lagoon. Intensive aeolian processes led to formation of sand dunes elongated wetland depressions. This has resulted in the current composition of the subgrade, composed primarily of spit/ aeolian sands with thin organic material interbeddings. For the above-mentioned LNG project full-containment type tanks were designed. They are built of two layers: the inner tank made of nickel steel to obtain the required resistance to low temperature cracking, which holds the liquefied gas and the outer casing tank made of prestressed concrete. The tanks have perlite/ glass fibre insulation system. The specific design of the tanks makes them very sensitive to uneven subsidence of subgrade material under their foundation.

The first option considered in the LNG Terminal project was deep foundation on piles. However, FEM calculations showed that it was actually possible to use foundation slabs instead. These should be made of cement-bound mixes of Young's modulus 400 MPa or higher. Thus, 0.55 thick prestressed concrete slabs were designed for the LNG tanks in question. The slab was placed on 1.75 m thick concrete base layer. Considering the critical nature of the project, extensive preliminary site examinations and tests were carried out to specify a concrete mix of appropriate E-modulus value. In addition, it should not pose construction problems during placement.

Based on the analysed properties of cement-bound mixes, a mix specified in the Polish guide for design of flexible and semi-rigid pavements was chosen of 28 day compressive strength in the range of 2.5-5.0 MPa. Its should have E-modulus value of 4,500 MPa before cracking, dropping to 300 MPa after cracking. The following three mixes were chosen for preliminary tests:

- Mix1 composed of 62.2% of 0/2 sand, 29.2% of 2/8 gravel, 4.9% of CEM III/a 32.5N and 3.7% of fly ash ,
- Mix2 composed of 91.6% of 0/2 sand, 4.7% of CEM III/A of 32.5N and 3.7% of fly ash ,
- Mix3 composed of 92.6% of 0/3 sand, 4.2% of CEM III/A of 32.5N and 3.2% of fly ash ,

The E-modulus and compressive strength values were determined experimentally on ϕ=150 mm and h =300 mm cylindrical samples made in 3-gang split design concrete cylinder moulds with top and bottom pieces. The compaction effort was 0.6 J/cm^3 ±10%. During the moulding process, samples for CBR and Proctor tests were taken. In the E-modulus and compressive strength test the

compressive stress increased at a rate of 0.6±0.4 MPa/m^{2}·s. On the cylinder side walls lines were marked to measure strain. Three measurements were carried out on these vertical lines spaced at 120° intervals around the side wall. (Fig. 1). The gauge length centre was located at half the height of the sample. The following procedure was applied in the E-modulus test:

- the sample was loaded up to compressive stress of σ_b= 0.05 MPa and the resulting strain ε_{b0} was measured
- the test load was increased up to σ_a=1/3 f_c, maintained for 60 s at that level, and after the next 30 s ε_{a0} was measured
- the sample was unloaded to stress level σ_b, which was maintained for 60 s and after the value of ε_{b1} was measured (Fig 2),
- this procedure was repeated at least 2 times,
- when all the required values had been determined, load was increased up to failure of the sample (Fig 3).

Fig. 1: Elastic modulus tester

Table 1 gives the results obtained on the tested mixes after seven days of curing

Mix No.	E_s [MPa]	ν [–]	f_c [MPa]
1	7,594	23.2	1.55
2	2,882	17.1	0.40
3	2,123	18.1	0.44

Mixes No. 1 and No. 2 were chosen for field testing based on the results of the preliminary laboratory tests. The trial construction sites were located at the planned tanks location. They were removed after the test. The compaction equipment used in the test was the same as in the future construction. The slabs were cast in 3 three lifts and 150/300 mm cylinders were cored after 7 days of curing (Fig. 4).

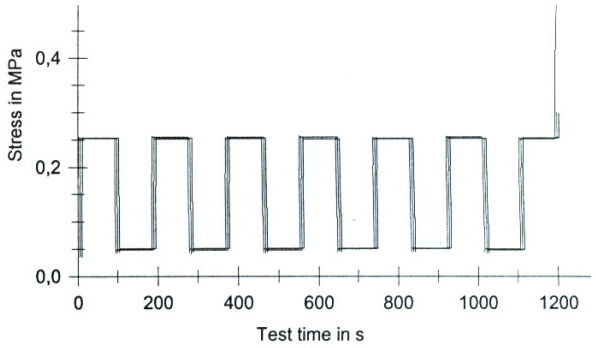

Fig. 2: Load increase over time during the E-modulus test

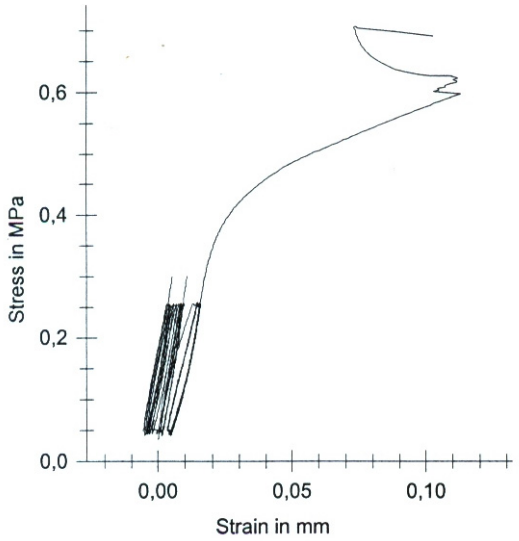

Fig. 3: Stress-strain plot of one of the tested mixes

Fig. 4: Trial construction site and coring of cylinders for E-modulus test

Finally, the construction supervision team and lead designers approved the Contractor's proposal to use Mix2 as a material for construction of the designed foundation slabs for the tanks in question.

ANALYSIS OF THE STRESS DISTRIBUTION AT A BI-MATERIAL INTERFACE

Lucie MALÍKOVÁ[1,2], *Mohammad Sami AL KHAZALI*[1,2], *Monika STŘEDULOVÁ*[1], *Stanislav SEITL*[1,2], *Jacek KATZER*[3]

[1] Faculty of Civil Engineering, Brno University of Technology, Veveří 331/95, Brno, Czech Republic
[2] Institute of Physics of Materials, Czech Academy of Sciences, v.v.i., Žižkova 513/22, Brno, Czech Republic
[3] Faculty of Geoengineering, University of Warmia and Mazury in Olsztyn, 10-720 Olsztyn, Poland

lucie.malikova@vut.cz, mohammad.al.khazali@vutbr.cz, monika.stredulova@vut.cz, seitl@ipm.cz, jacek.katzer@uwm.edu.pl

At present, 3D printing is the best known and disseminated additive manufacturing technology. Although metals and concrete increase their popularity, different polymers are still the most popular materials for this technology. Thus, 3D printing of polymer reinforcement for concrete becomes more popular, which is connected to the fact that the development of traditional steel reinforcement for concrete structures reached its technological limits. Lower strength and modulus of elasticity of 3D printed polymers in comparison to steel can be compensated by the possibility of creation of a very complicated spatial shape to reinforce the concrete structure [1].

A simplified geometry of a rectangular concrete specimen (40 × 40 × 160 mm) reinforced by a triangular polymer part of various height H (0, 5, 10, 15 and 20 mm) subjected to both three-point-bending and pure bending has been modelled via finite elements, see a scheme in Fig. 1, and the stress distribution at selected places was investigated. Young's modulus and Poisson's ratio for concrete and polymer were 20 GPa and 0.2 and 2 GPa and 0.4, respectively. The main goal was to compare the results of the numerical simulations with experimental data obtained from both static and cyclic tests, see an example of a broken specimen in Fig. 2. The tested specimens break in a specific manner in some cases and the finite element simulations should help to understand if there is some reason for such kind of failure. Stress tensor components as well as principal and von Mises stresses were analysed.

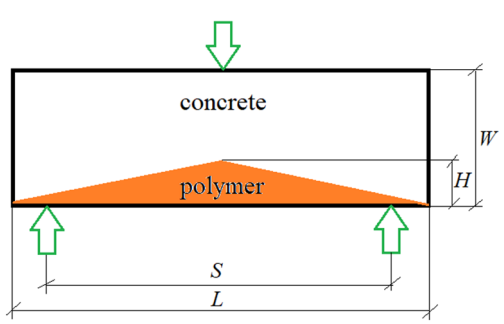

Fig. 1: Scheme of the rectangular concrete polymer reinforced by a polymer part at the bottom subjected to three-point-bending.

Fig. 2: An example of a broken reinforced concrete specimen.

The stress distribution especially at the interface between the concrete and polymer (which is probably the most important place regarding the results of the experiments) obtained for various reinforcement height was compared and the results were discussed thoroughly. The dangerous location appears above the both supports during the 3-point-bending test.

Acknowledgements

This paper was created as a part of the project No. CZ.02.01.01/00/22_008/0004631 "Materials and technologies for sustainable development" within the Jan Amos Komensky Operational Program financed by the European Union and from the state budget of the Czech Republic. Financial support from the Faculty of Civil Engineering, Brno University of Technology (project No. FAST-S-24-8503) is also gratefully acknowledged.

References

[1] KATZER, J. and T. SZATKIEWICZ. Properties of concrete elements with 3-D printed formworks which substitute steel reinforcement. *Construction and Building Materials*. 2019, vol. 210, pp. 157–161. DOI: 10.1016/j.conbuildmat.2019.03.204.

EVALUATION OF THE CHLORIDE CONTENT IN WASTE AGGREGATE CONCRETE BY X-RAY FLUORESCENCE

Kateřina MATÝSKOVÁ[1], *Marie HORŇÁKOVÁ*[2]

[1] Department of Materials, Faculty of Civil Engineering, VSB Technical University of Ostrava, Ludvíka Podéště 1875/17, 708 33 Ostrava-Poruba, Czech Republic
[2] Department of Structural Mechanics, Faculty of Civil Engineering, VSB Technical University of Ostrava, Ludvíka Podéště 1875/17, 708 33 Ostrava-Poruba, Czech Republic

katerina.matyskova@vsb.cz, marie.hornakova@vsb.cz

Chloride ingress is a significant concern in concrete structures, particularly in environments where chloride ions can lead to corrosion of reinforcement, thereby jeopardizing structural integrity. Thus, the determination of chloride content in concrete is crucial for predicting the probability of rebar corrosion. Classical methods, such as argentometric titration, potentiometric measurements, and atomic absorption, provide precise results but are time-consuming, especially for large structures. Alternative techniques, such as electrical conductance measurement and colorimetric tests, offer estimations of chloride penetration resistance but lack quantitative evaluation of chloride concentration. X-ray fluorescence (XRF) emerges as a promising analytical method for determining chloride content in concrete structures. XRF (Fig. 1) allows for a greater number of measurements in a shorter time frame compared to classical methods, making it suitable for large-scale measurement campaigns.

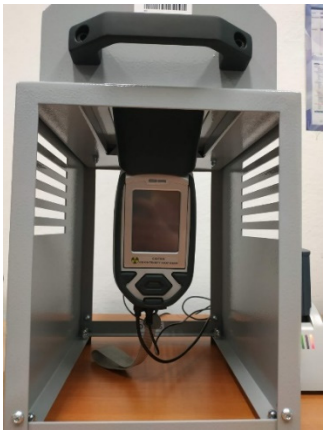

Fig. 1: XRF tool

This study focuses on the evaluation of chloride content in structural lightweight waste red ceramic fine aggregate concrete. Concrete powder was drilled from a 168-day old sample that had been exposed to chloride ions in aqueous solution for 90 days in accordance with natural bulk chloride test NT Build 443. 1 gram of the concrete powder was analyzed three times by using handheld XRF analyzer gun (Thermo Fisher Scientific XRF- NITON XL3t 980 GOLDD).

The results obtained by XRF analysis are compared to the results measured by scanning transmission electron microscope with EDS microanalyzer (EDX). Therefore, 1 gram of powder was also analyzed by a scanning electron microscope JEOL JSM-7610F Plus (JEOL, Japan) in vacuum. The results of the first drilled layer from the sample are given in Fig. 2.

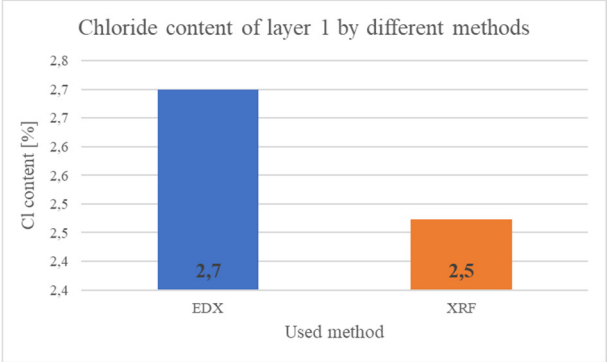

Fig. 2: Results of measurements.

The results demonstrate a substantial correspondence between XRF and EDX measurements. Both methodologies operate on a similar principle; however, XRF provides greater information depth, whereas EDS may yield diverse outcomes on an uneven surface due to its smaller irradiation area.

It should be noted that a comparison with classical chemical analysis would also be useful to determine the efficiency of the measurements. The chemical titration analysis of chloride ions in hardened concrete can be carried out in accordance with the methodology given in standard EN 14629. However, it is worth mentioning that the outcomes of the titration test are expressed in weight percentage, whereas non-destructive XRF methods yield results as a percentage of the analyzed surface.

Acknowledgements

The research was funded by the Ministry of Education, Youth and Sports of the Czech Republic through VSB – Technical University of Ostrava (SGS SP2024/097).

NUMERICAL MODELLING OF WATER MIST DISPERSION DUE TO TRAFFIC

Ivan KOLOŠ[1], *Vladimíra MICHALCOVÁ*[1] *and Lenka LAUSOVÁ*[1]

[1]Department of Structural Mechanics, Faculty of Civil Engineering, VSB – Technical University of Ostrava, Ludvíka Podéště 1875/17, Ostrava-Poruba, Czech Republic

ivan.kolos@vsb.cz, vladimira.michalcova@vsb.cz, lenka.lausova@vsb.cz

The transport structures are exposed to a large amount of road salt during the winter, which causes them to suffer corrosion-related damage. The aim of this study is to analyze the transport of water mist sprayed from the road to the near and far surroundings by passing vehicles in different wind directions.

Modeling was done in ANSYS Fluent software. The computational domain was divided into 3 zones (Fig. 1): preparation zone (60 m long), analytic zone (90 m long), exit zone (30 m long). Sliding with simplified model of the truck passes through all 3 zones.

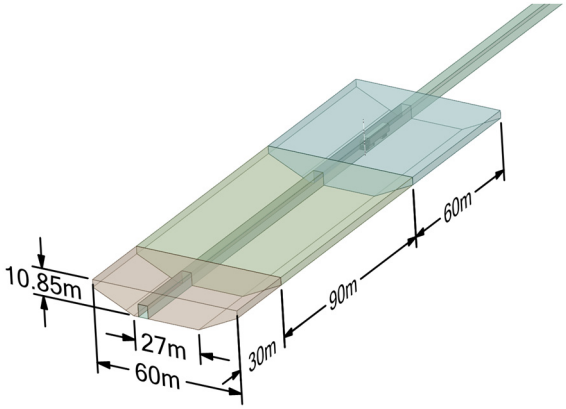

Fig. 1: Computational domain divided into zones.

Boundary conditions:

Vehicle speed 25 m/s, wind speed 20 m/s. Considered wind directions + and - 60° from the x-axis in the horizontal plane, against the direction of movement of the vehicle. Standard k-epsilon turbulent model including wall functions is used to model wind flow. Discrete phase is modeled by Euler-Lagrange approach.

Preliminary study calculations have shown that the detailed modelling of droplet spraying by the entry of a rotating wheel into the liquid layer is inefficient due to the scale of the task, with excessively high demands on computing power. Therefore, a simplifying model was considered, where particles are injected from sidewalls of tires. Inert particles of constant diameter $2.5e^{-5}$ m, total flow rate 4.5 kg/s (based on [1]), particle initial velocity 25 m/s (Fig. 2).

The boundaries of the domain are based on the real geometry of the nearby road, on which probes are installed to measure the amount of chloride deposits [2].

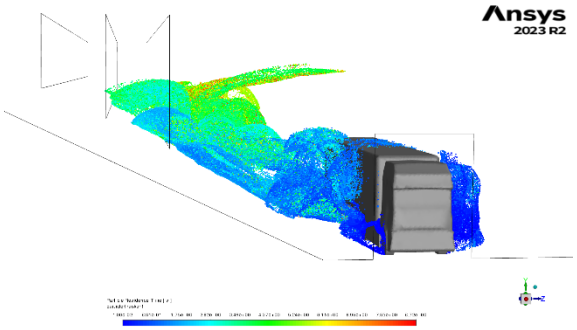

Fig. 2: Aerosol wake behind a passing truck. Wind 20 m/s and angle 60°.

Acknowledgements

This contribution has been developed as a part of the research project GACR 22-19812S "Effect of gaseous and traffic induced pollutants on the durability of selected construction materials" supported by the Czech Science Foundation.

This work was supported by the Ministry of Education, Youth and Sports of the Czech Republic through the e-INFRA CZ (ID:90254).

References

[1] LOTTES, S.A. and C. BOJANOWSKI. *Computer Modeling and Analysis of Truck Generated Salt spray Transport Near Bridges. Argonne National Laboratory*. DOI: 10.2172/1087817

[2] VACEK, M., V. KŘIVÝ, K. KREISLOVÁ, M. VLACHOVÁ and M. KUBZOVÁ. Experimental Measurement of Deposition Chloride Ions in the Vicinity of Road Cut. *Materials 2023, Vol. 16, Page 88*. **16**(1), 88. DOI: 10.3390/MA16010088

CORROSION AND MATERIAL ANALYSIS OF PRESTRESSED TENDONS FAILURE FROM COLLAPSED ROOF STRUCTURE

Petr MYNARČÍK[1], *Miroslav VACEK*[2]

[1] Centre for Building Experiments and Diagnostics, Faculty of Civil Engineering, VSB - Technical university of Ostrava, Ludvika Podeste 1875/17, Ostrava, Czech Republic
[2] Department of Structures, Faculty of Civil Engineering, VSB - Technical university of Ostrava, Ludvika Podeste 1875/17, Ostrava, Czech Republic

petr.mynarcik@vsb.cz, miroslav.vacek@vsb.cz

Structural failures and collapses are potential terminations of building structures lifetime. Corrosion is one of the most damaging and costly naturally occurring process. This article presents authentic facts about partial roof collapse during December 2023. Fortunately, without loss of life, but with serious property damage. Neglected maintenance of roof sheathing allowed flow of rainwater into the anchor areas of the prestressed roof trusses. Corrosion slowly but surely worked on prestressed tendons disruption for dozens of years. Roof debris provided numerous samples for more detailed material analysis.

Fig. 1: Collapsed roof structure - December 2023, Czech Republic

The presented research dealt with the implementation of a very precision 3D scanning of the original test samples of prestressing tendons. Scanning was performed using a high-resolution profilometer. Subsequently, the samples were exposed to a simulation of the corrosion environment in the corrosion chamber. Increased temperature and salt spray test were used to accelerate corrosion processes. The disturbed samples were scanned again to compare the surface corrosion damage with initial 3D scans. The next step was performing a tensile testing of the material of interest. The final analysis consisted of finding the failure locations on the test samples and comparing them with their precision 3D models.

Fig. 2: Fragments of corroded prestressed tendons

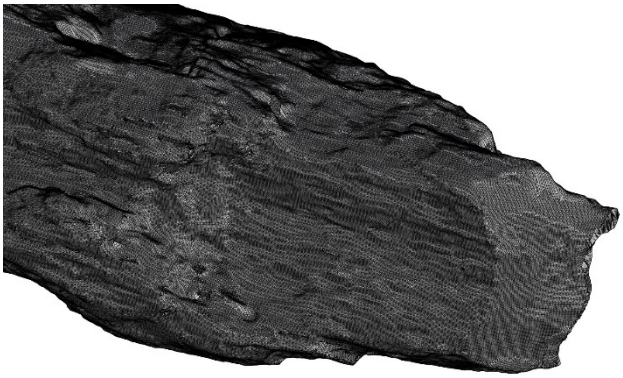

Fig. 3: High precision profilometric 3D scan of prestressed tendon

Acknowledgements

The applied research was funded by commercial contract No. HS2072405 "Experimental verification of the confocal microscopy method applicability for assessing corrosion damage of prestressing reinforcement in situ." Purchaser: Rada Building s.r.o. Especial acknowledgments to SVÚOM s.r.o. for enabling to use microscopic equipment.

ANALYSIS OF ROTATIONAL STIFFNESS OF SELECTED END-PLATE JOINTS OF STEEL BEAMS USING THE ARAMIS OPTICAL SYSTEM

Przemysław PALACZ[1], *Maciej MAJOR*[2]

[1] Czestochowa University of Technology, Faculty of Civil Engineering, Akademicka 3 Street, 42-200 Czestochowa, Poland

[2] Czestochowa University of Technology, Faculty of Civil Engineering, Akademicka 3 Street, 42-200 Czestochowa, Poland

przemyslaw.palacz@pcz.pl, maciej.major@pcz.pl

In individual steel structures, individual elements are required to be connected. For this purpose, we distinguish several types: welded, screwed, riveted and glued [1]. Bolted connections are an indispensable element of every steel structure, activated by simple and quick assembly of structural elements on the construction site. [2].

The basic parameter classifying the connection is rotational stiffness, which depends on the stiffness of the connection. The stiffness of a connection is influenced primarily by the geometry of all components, including bolts and adjacent connected elements. The compliance characteristics can be determined from the relationship between the bending moment in its rotation report, i.e. by the M-ϕ curve.

In the article regarding rotational stiffness controls of selected end-plate joints of the ARAMIS SRX non-contact operating system. The measuring equipment consists of two cameras recording images with a frequency of up to 500 seconds. The measuring station is shown in Fig. 1.

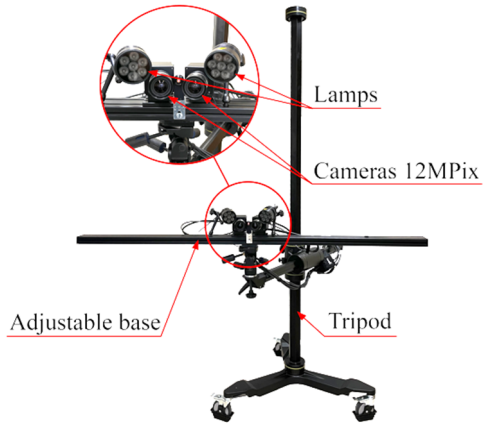

Fig. 1: ARAMIS SRX measuring system.

The measurement is performed using the photogrammetry principle, i.e. the coordinates of the sample points are determined based on the photos taken. First, a reference photo of the sample in its unshaped state is taken, and then a series of photos corresponding to the next stages of the test are taken. Then, the program analyzes the coordinates of the points and, on this basis, determines the position of the points relative to the reference photo. Measuring points can be implemented using special stickers glued to the sample or special painting on the sample in the form of an irregular pattern. Based on the measured displacements of the connection point coordinates, the rotational stiffnesses of the tested connections were determined. Fig. 2 shows the test results for point coordinate displacement tests.

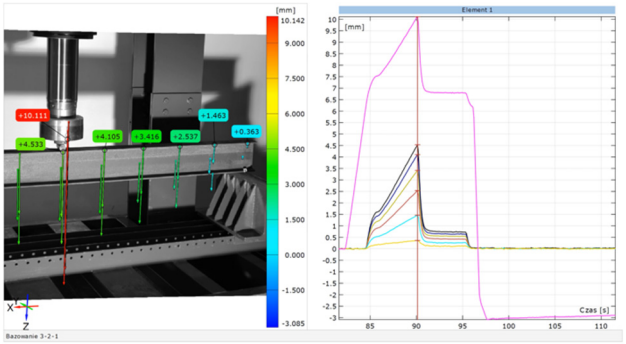

Fig. 1: Graph of displacements of measurement points of the tested sample.

References

[1] M.J. Kontoleon, D.N. Kaziolas, M.D. Zygomalas, C.C. Baniotopoulos, Analysis of steel bolted connections by means of a nonsmooth optimization procedure, Computers & Structures, Volume 81, Issues 26–27, 2003, Pages 2455-2465.

[2] P. Chen, F. Gao, J. Wan, Experimental and numerical study of the tensile behavior of high-strength steel T-stub, Progress in Steel Building Structures, 2022.

ANALYSIS OF THIN-WALLED CROSS-SECTION IN COMBINED LOADING

Přemysl PAŘENICA[1], *Jakub FLODR*[2], *Markéta PASTRNKOVÁ*[3]

[1,2,3] SSI SCHÄFER s.r.o., Tovární 325, Hranice, Czech Republic

premysl.parenica@ssi-schaefer.com, jakub.flodr@ssi-schaefer.com, marketa.pastrnkova@ssi-schaefer.com

The subject of the extended abstract is a comparison of selected methods for the design of the undercarriage of a cantilever mobile racking system. The system consists of a chassis part that takes care of the movement on the rails system. The racking part is connected to the undercarriage and is used for storage (Fig. 2). The chassis part is composed of a double thin-walled U-profile, which is transversely connected by stiffeners, shafts, and end plates. In the middle section, the beams are connected by a bolted detail of the cantilever rack column.

In this paper, attention is paid to the analysis and comparison of possible computational approaches for the design of a pair of thin-walled chassis beams. Three independent numerical methods were selected for comparison.

The basic numerical model was created using a 3D member model, where torsion effects are considered in the assessment using elements with 7 DOF. With this method, it is possible to consider the influence of imperfections from the cross-section plane. The second numerical model is created in the IDEA StatiCa Member software, where a relatively detailed shell model is already created, including an idealized support of shafts, bolted connections, stiffeners, and detail of the support of the column in the middle part. The last model is a validation model and is created in ANSYS using shell elements and considering the idealized details of the connections. This model offers a comprehensive view of the problem at hand. The aim is to compare the different numerical analysis methods and determine the resulting capacity of the chassis structure.

The evaluation methodology is chosen concerning the conciseness of the results for the available chassis variants. The geometric dimensions of the models are parametrically defined. The variable dimensions are the length of the chassis and the height of the double U profile. Based on the parametric study on the 3D member model, a matrix of variants is developed, which is further performed on the detailed shell models.

The comparison is made from the point of view of stress analysis of chassis beams. The stress analysis on the basic numerical member models is evaluated at the elastic design level. More sophisticated numerical shell models can be further evaluated at the level of plastic design level to determine the ultimate capacity [1].

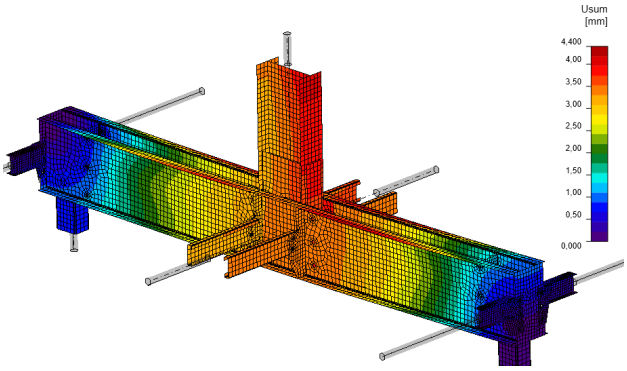

Fig. 1: Numerical model of chassis in IDEA StatiCa Member.

A fundamental issue is the correct choice and interpretation of imperfections and their application within the individual approaches. In particular, the application of imperfections when using the 7 DOF design method is specific.

Fig. 2: Chassis part with connection to the rack building.

References

[1] ČSN EN 1993-1-5 ed. 2 (731401) A Eurokód 3: Navrhování ocelových konstrukcí. ÚNMZ, 2013.

RELIABILITY-BASED PROBABILISTIC ELASTO-PLASTIC TOPOLOGY OPTIMIZATION OF STRUCTURES

Majid Movahedi RAD[1,*], *Muayad HABASHNEH*[1], *János LÓGÓ*[2]

[1] Department of Structural and Geotechnical Engineering, Széchenyi István University, H-9026 Győr, Hungary
[2] Department of Structural Mechanics, Department of Highway and Railway Engineering, Budapest University of Technology and Economics, H-1111, Budapest, Hungary

majidmr@sze.hu, muayad.habashneh@sze.hu, logo.janos@emk.bme.hu

In this research, a novel approach to topology optimization is proposed which integrates considerations of uncertain load positions, thereby enhancing the reliability-based design within the context of structural engineering. By extending the conventional framework to encompass imperfect geometrically nonlinear analyses, this research discovers the intricate interplay between nonlinearity and uncertainty, shedding light on their combined effects on probabilistic analysis. A key innovation lies in the treatment of load position as a stochastic variable, augmenting the existing parameters such as volume fraction, material properties, and geometric imperfections to capture the full spectrum of variability inherent in real-world conditions. To address these uncertainties, normal distributions are adopted for all relevant parameters, leveraging their simplicity, ease of implementation, and computational efficiency, particularly crucial in the context of complex optimization algorithms and extensive analyses.

Methods

The presented methodology for topology optimization takes into account initial geometrical imperfections and probabilistic design, which makes it more realistic and robust. This approach ensures that the structures designed through our methodology can adapt better to unpredictable conditions in the real design. The objective function for the topology optimization problem is formulated as follows:

$$Minimize: C = u^T K u \tag{1}$$

The denotation K refers to the global stiffness matrix. The mean compliance is represented by the denotation C. The displacement of the system is represented by u.

When designing for reliability, we take into account various factors such as the location of the load, material properties, geometric imperfections, and volume fraction, all of which are treated as random variables that follow a normal distribution with mean values and standard deviations. Our methodology places great importance on the reliability constraint outlined in Eq.(2), which is tied to the volume fraction. This constraint not only establishes a crucial link between the targeted (β_{target}) and calculated reliability index (β_{calc}) but also guarantees that our optimization process meets strict reliability standards, ultimately resulting in stronger, safer structures.

$$\beta_{target} - \beta_{calc} \leq 0 \tag{2}$$

This approach takes into account the concept of the plastic limit ultimate load multiplier. This critical aspect is carefully integrated to consider the complex interaction between material plasticity and structural stability. The related constraint is constructed as follows:

$$m_s - m_p \leq 0. \tag{3}$$

The load multiplier is represented by the numeric value m_s, while the plastic ultimate load multiplier is denoted by m_p.

The methodology relies on the fundamental constraints of the bi-directional evolutionary structural optimization (BESO) method, which are outlined in Eqs. (4), (5), and (6). These constraints are crucial for deterministic designs and address key considerations related to volumes and binary design variables, forming the basis for the optimization process. In the case of probabilistic designs, Eq. (2) is also employed.

$$V^* - \sum_{i=1}^{N} V_i x_i = 0 \tag{4}$$

$$\frac{V^*}{V_0} - V_f \leq 0 \tag{5}$$

$$x_i \in \{0,1\} \tag{6}$$

Here, V_i represents the volume of each element within a structure, while V^* represents the overall volume of the structure. The number of elements is denoted by N, and the volume of the design domain is represented by V_0. Additionally, V_f denotes the proportion of volume fraction.

EVOLUTION OF LONG-TERM STRENGTH AND SHRINKAGE STRAIN IN SEAWATER-MIXED CEMENTITIOUS SYSTEMS

Sundar RATHNARAJAN[1], *Pawel SIKORA*[1]

[1] Faculty of Civil and Environmental Engineering, West Pomeranian University of Technology in Szczecin, Poland

sundar.rathnarajan@zut.edu.pl, pawel.sikora@zut.edu.pl

The use of potable or fresh water (FW) in the production of raw materials and the mixing of concrete can increase the water stress in regions facing water scarcity [1] The inclusion of supplementary cementitious materials (SCMs) and alternative reinforcements in concrete can facilitate the use of non-potable waters in concrete production [2]. Seawater and sea sand (SW-SS) concretes have been extensively researched in recent times to understand the fundamental mechanisms of hydration and the strength development of the same [3]. However, limited information is available on the long-term strength and shrinkage strain development of SW-SS concretes produced with SCMs. Current work focuses on evaluating the compressive strength and total unrestrained shrinkage strain in seawater-mixed (SW) cementitious systems.

A total of 20 mixes (10 FW and 10 SW-mixed) of concrete were produced with binary and ternary-blended binder compositions using fly ash, slag, and metakaolin as SCMs, along with CEM I 42.5 R. Concrete cubes of size 100 mm were produced and cured in under-water immersion for a period of 28 days. The compressive strength of the concrete was measured at 7, 28, and 90 days according to EN 12390 – Part I. Similarly, mortar prisms of dimension 40×40×160 mm were produced using the above-mentioned compositions, and the unrestrained shrinkage of these specimens was measured using the Grauf-Kaufmann method. The shrinkage values were measured for up to 90 days to assess the variations in shrinkage strain between FW and SW-mixed mortars.

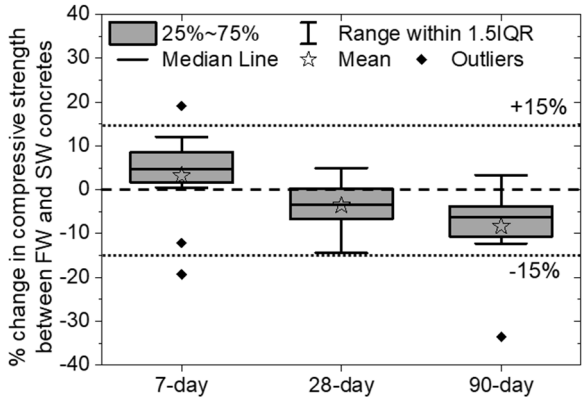

Fig. 1: Evolution of percentage change in compressive strength between FW and SW-mixed concretes over time

Fig 1 shows the evolution of percentage change in strength between FW and SW concretes. Up to 28 days there is no significant reduction in compressive strength compared to the 90th day strength. Even at 90 days the box plot values indicate that the median value of reduction in strength of concretes was lesser than 15%.

Fig 2 shows the total shrinkage strain between FW and SW-mixed mortars at 90 days. In general, a significant increase in the total unrestrained shrinkage strain of SW-mixed mortars is observed. MF30 mix, a binary combination of fly ash added mix showed a significantly higher shrinkage strains compared to other mixes.

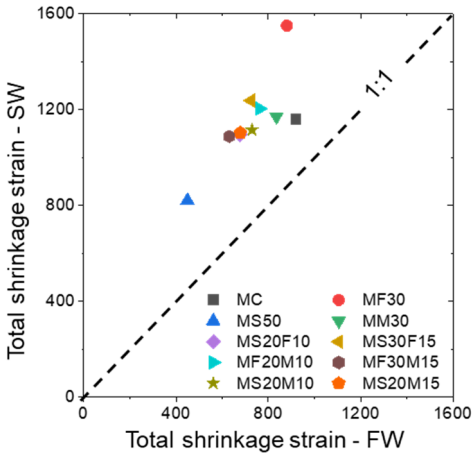

Fig. 2: Influence of SW-mixing on unrestrained total shrinkage of cementitious systems

Acknowledgements

This research is part of the project No. 2021/43/P/ST8/00945 co-funded by the National Science Centre and the European Union Framework Program for Research and Innovation Horizon 2020 under the Marie Sklodowska-Curie grant agreement No. 945339.

References

[1]. Ding C, Dong W, Zhang A, et al (2021) Life cycle water footprint assessment of concrete production in Northwest China. Water Policy 23:1211–1229.

[2]. Rathnarajan S, Sikora P (2023) Seawater-mixed concretes containing natural and sea sand aggregates – A review. Results in Engineering 20:101457.

[3]. Ebead U, Lau D, Lollini F, et al (2022) A review of recent advances in the science and technology of seawater-mixed concrete. Cem Concr Res 152:

ELEVATED TEMPERATURE PERFORMANCE OF 3D PRINTED CONCRETE CONTAINING SILICA-COATED BISMUTH OXIDE/GADOLINIUM OXIDE PARTICLES

Pawel SIKORA[1], *Szymon SKIBICKI*[1], *Krzysztof CENDROWSKI*[1], *Mateusz TECHMAN*[1], *Karol FEDEROWICZ*[1], *Daniel SIBERA*[1]

[1] Faculty of Civil and Environmental Engineering, West Pomeranian University of Technology in Szczecin, Poland

pawel.sikora@zut.edu.pl

This study aims to evaluate the performance of 3D printed concrete (3DPC) after exposure to elevated temperatures of 450, 600, and 750 °C. For this purpose, both cast and printed specimens were prepared. In addition to plain (reference) 3D printed concrete specimens, two additional concrete mixes containing heavy-weight radiation shielding admixtures (namely bismuth oxide – Bi_2O_3 and gadolinium oxide – Gd_2O_3 nanoparticles) were evaluated. The first mix was modified with pristine Bi_2O_3/Gd_2O_3 particles at a mass ratio of 1:1. The second mix was modified with silica-coated Bi_2O_3/Gd_2O_3 (mass ratio 1:1), following the methodology presented in [1] and shown in Figure 1. In the modified 3DPC mixes, cement was replaced with 2.5 vol% of nanoparticles.

The experimental protocol included evaluations of density loss, dynamic elastic modulus, flexural strength, and compressive strength. Additionally, visual inspections of the specimens were performed.

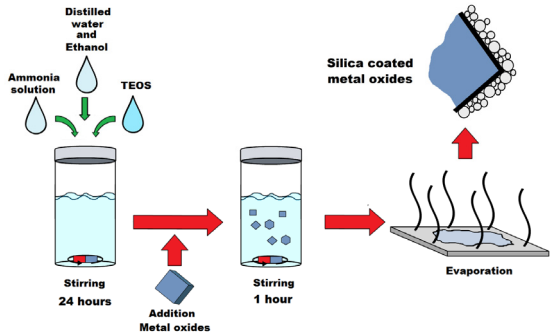

Fig. 1: Schematic representation of silica-coating on the surface of Bi_2O_3 and Gd_2O_3 nanostructures [1]

Exposure of the specimens to elevated temperatures resulted in their gradual deterioration, with distinct differences observed between cast and printed specimens. Elevated temperatures led to a noticeable decrease in both the dynamic elastic modulus and the overall mechanical performance of the specimens. Up to 450 °C, no surface cracking was reported. However, exposure to temperatures of 600 °C and 750 °C resulted in debonding within the interlayer zones of the 3D printed specimens. In contrast, the cast specimens exhibited only minimal surface cracking. Exposure to a temperature of 450 °C resulted in an average decrease in the dynamic elastic modulus of the specimens by 45%, while after exposure to 750 °C, the dynamic elastic modulus value decreased by approximately 85% in all tested specimens.

Regarding the mixture modification with nanoparticles, a slight increase in density was reported, while no distinct differences in the performance of the specimens after exposure to elevated temperatures were observed. Therefore, it can be concluded that radiation shielding admixtures exhibit a marginal influence on the thermal performance of 3D printed concrete (3DPC).

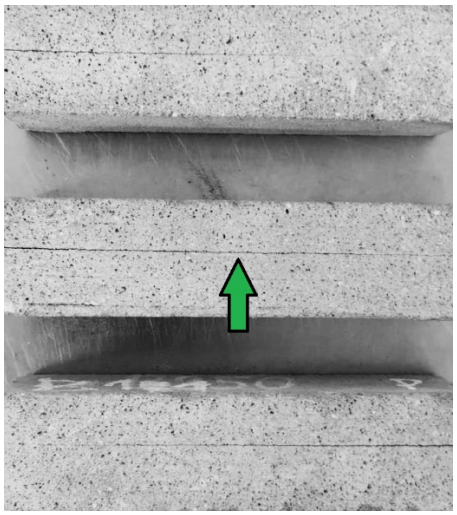

Fig. 2: Example on inter-layer debonding of specimens after exposure to 750 °C

Acknowledgements

This research was funded in whole by the National Science Centre, Poland within Project No. 2020/39/D/ST8/00975 (SONATA-16).

References

[1]. Cendrowski K, Federowicz K, Techman M, Chougan M, El-Khayatt A.M., Saudi H.A, Kędzierski T, Mijowska E, Strzałkowski J, Sibera D, Abd Elrahman M, Sikora P (2024) Functional Bi_2O_3/Gd_2O_3 silica-coated Structures for improvement of early age and radiation shielding performance of cement pastes. Nanomaterials 14(2), 168.

STRENGTH OF MAGNETIC IRON-MIXED PLA FOR 4D PRINTING APPLICATIONS

Viet Hung TRAN[1], *Jakub MESICEK*[2,*], *Quoc-Phu MA*[2], *Ngoc Huynh Nhu NGO*[3], *Jana PETRU*[2]

[1] Faculty of Information Technology, Ho Chi Minh city University of Industry and Trade
[2] Department of Machining, Faculty of Mechanical Engineering, Technical University of Ostrava, Ostrava, Czech Republic
[3] Department of Chemistry Engineering, Ton Duc Thang University
jakub.mesicek@vsb.cz

The burgeoning field of 4D printing, spurred by the advancements in 3D printing technology, holds significant promise across various domains such as smart materials, civil and mechanical engineering, medicine, and automation. In view of this, the strength characterization of the 4D printed materials becomes essential for modern research.

In this study, we delve into the characterization of polylactic acid (PLA) filament infused with approximately 40% iron powder. Two sets of samples—traditional PLA and PLA/Fe—were fabricated using a popular commercial 3D printer employing fused deposition modeling (FDM) under identical printing conditions. We refer to the ASTM D638, D785, and D790 for the sample designs. The specimens were printed on desktop FDM printer (Prusa i3 MK3S) within the printing volume of 330 mm×270 mm×200 mm. The printing parameters are listed in **Tab.1**. The shape of the samples can be observed in **Fig.1**.

Tab. 1: Printing parameters.

Infill	100%
Layer height [mm]	0.2
Print speed [mm/s]	50
Extruder temperature [°C]	215
Bed temperature [°C]	60

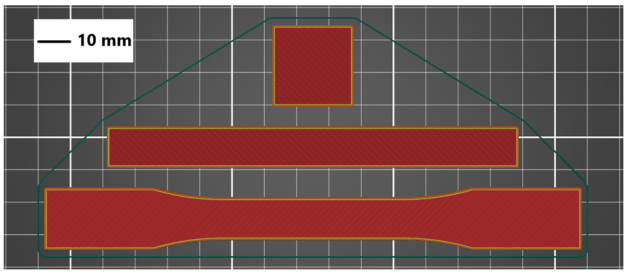

Fig. 1: From top to bottom, the samples for testing hardness, flexural strength, and tensile strength.

Our investigation focuses on discerning the disparities between PLA and PLA/Fe concerning material properties including tensile strength, flexural strength, hardness, and fracture surface characteristics. The comprehensive analysis of our findings reveals that traditional PLA exhibits superior mechanical properties compared to PLA/Fe, encompassing higher tensile strength, flexural strength, hardness, and modulus. Consequently, our study underscores the necessity for further exploration into PLA/Fe materials to ascertain their viability as magnetic filaments for robust 4D printed products in real-world applications.

The experimental results are reported in **Tab.2**.

Tab. 2: Test results.

Properties	PLA	PLA/Fe
Tensile strength [MPa]	57.80 ± 0.49	32.58 ± 0.39
Tensile modulus [MPa]	1919.6	1703.8
Elongation at break [mm]	2.79 ± 0.21	3.06 ± 0.24
Flexural strength [MPa]	19.24 ± 0.41	15.45 ± 0.77
Flexural Modulus [GPa]	3.326	3.318
Deflection at flexural strength [mm]	99.22 ± 1.50	69.76 ± 02.13
Hardness – shore D	84	81

The experiments showed that the mechanical properties of PLA/Fe printed products were considerably weaker in comparison with traditional PLA printed products. This effect is likely owing to the high per-centage (i.e. 40%) of iron particles in Proto-Pasta PLA/Fe filament.

Acknowledgements

This article was funded by the European Union under the REFRESH—Research Excellence For REgion Sustainability and High-tech Industries project number CZ.10.03.01/00/22_003/0000048 via the Operational Programme Just Transition.

Využití Breslovy metody pro stanovení depoziční rychlosti chloridových iontů

Miroslav VACEK[1], *Vít KŘIVÝ*[1]

[1]Fakulta stavební, VŠB – Technická univerzita Ostrava, Ludvíka Podéště 1875/17, Ostrava - Poruba

miroslav.vacek@vsb.cz, vit.krivy@vsb.cz

Korozní poškození ocelových a železobetonových konstrukcí je závislé na prostředí, ve kterém se stavební objekt vyskytuje. V současnosti jsou hlavní korozní stimulanty staveb v okolí silničních komunikací chloridové ionty. Znečištění chloridy je na konstrukce zanášeno především v zimním období, kdy probíhá údržba sjízdnosti silničních komunikací chemickými rozmrazovacími látkami ve formě posypové soli (nejčastěji NaCl) nebo roztoku soli (tzv. solanka). Projíždějící automobily deponují vodu ze silnice ve formě aerosolu a zvířeného prachu obsahujícího chloridové ionty, které se následně usazují na površích konstrukcí.

Metodika měření depoziční rychlosti chloridových iontů je popsána v normě ISO 9225. S využitím normalizovaných metod je možné měřit depoziční rychlost chloridových iontů v lokálním mikroklimatu.

Vyvíjená metodika měření depoziční rychlosti chloridových iontů pomocí Breslovy metody (měření probíhá dle ISO 8502-6 a ISO 8506-9) je motivována cílem autorů zjišťovat depoziční rychlost Cl^- iontů v závislosti na lokálních činitelích, jako je například konstrukční uspořádání detailů, orientace povrchu konstrukčního dílce atp. Za tímto účelem probíhá paralelní měření na experimentálních stojanech pro stanovení depoziční rychlosti chloridových iontů (dle ISO 9225). Na experimentální stojany byly osazeny kupóny v horizontální orientaci pro analýzu povrchu po měsíční expozici a ve vertikální orientaci pro měsíční a kumulativní expozici, viz obrázek 1.

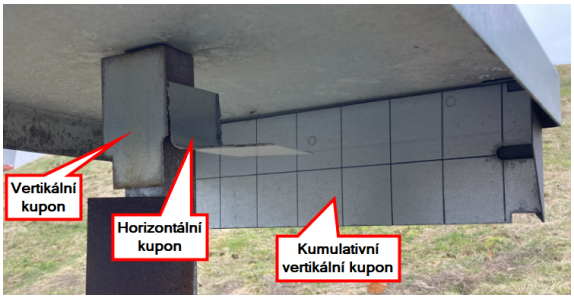

Obr. 1: Umístění kuponů - Breslova metoda

výsledkem měření Breslovou metodou je množství usazené soli na ploše. Tento údaj však nepostihuje časovou jednotku. Pro účely tohoto textu je uvážení času provedeno dle následujícího vztahu:

$$S_{d,b} = \rho_A / t \tag{1}$$

kde je

- $S_{d,b}$ - celková plošná hustota rozpustných solí na povrchu přepočtená na jeden den $(mg/(m^2 * den)$,
- ρ_A - celková plošná hustota rozpustných solí na povrchu stanovená Breslovou metodou (mg/m^2),
- t - časový údaj (den).

Koeficient determinace R^2 lineární regresní analýzy měření salinity svislého povrchu za den $(S_{d,b})$ a depoziční rychlosti stanovené metodou mokré svíce ($S_{d,c}$ dle ISO 9225) je na přijatelné hodnotě, viz obrázek 2. Statistická analýza je provedena na 35 vzájemných měřeních na vertikálním měsíčním kuponu a stanovení depoziční rychlosti metodou mokré svíce.

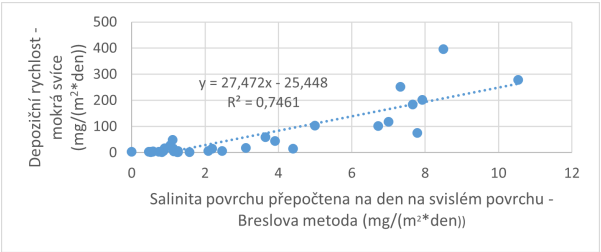

Obr. 2: Lineární regresní analýza salinity svislého povrchu za den a depozižní rychlost chloridových iontů stanovená metodou mokré svíce

Poděkování

Práce byly podporovány z prostředků Studentské grantové soutěže VŠB-TUO. Registrační číslo projektu je SP2024/058.

PLATE LOAD TEST OF SIMULATION MASS

Veronika VALAŠKOVÁ[1], *Jozef VLČEK*[2]

[1] Department of Structural Mechanics and Applied Mathematics, Faculty of Civil Engineering, University of Zilina, Univerzitna 8215/1, 010 26 Zilina, Slovakia
[2] Department of Geotechnics, Faculty of Civil Engineering, University of Zilina, Univerzitna 8215/1, 010 26 Zilina, Slovakia

veronika.valaskova@uniza.sk, jozef.vlcek@uniza.sk

Traffic is an important and integral part of our daily life. The large number of heavy vehicles on roads requires to deal with their negative effects. A vehicle moving along a roadway has static and dynamic effects on the pavement and nearby structures. Solving the given problem on real structures and vehicles is very time and cost consuming. As one separable part of the solution to this problem, the application of the small-scale physical modelling can give reliable results. Proposed approach can be applied in the laboratory. Small-scale physical modeling brings benefits, such as model size reduction, simplification, or controlled conditions during the test [1]. Based on the suitability and expediency of modeling on a reduced scale, we decided to perform experimental and numerical analysis of the static plate load test on the simulation mass which represents a pavement subgrade.

The presented work solves this task from static point of view. On the real structures, a numerous variations of static testing can be applied. On the physical model, a standard plate load test was performed. The static plate load test with the diameter of 60 mm was completed in 5 measurement stages. The circular plate was characterized by its rigidity and lightness. The measured values were subtracted from digital indicators. The equipment was installed on the rigid frame. Each stage was performed for period of 30 seconds.

In every stage, the load was measured and the peak value of modulus of elasticity was calculated. Results were in interval from 269.8 Pa to 319.2 Pa which is in good agreement with previous research.

The deformation amplitudes correspond with the FEM modelling outputs based on linear elastic material model. The loading and unloading phase of the stage was almost identical. Peak values of vertical loads were in the interval from 2.0 to 3.6 kg. There was an assumption of the small increment of mass deformation because of the weight of the loading mechanism apparatus. The selection of the appropriate modulus depends on the loading mode applied to the soil body and related load-deformation curve segment represented by the interval of contact stress. Short-term cases require high moduli values because of short-time influences on the soil body such as response during seismic events or dynamic excitation.

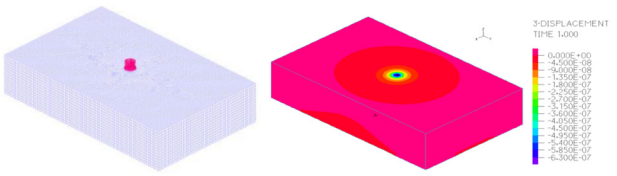

Fig. 1: FEM model of mesh, displacements in the numerical model

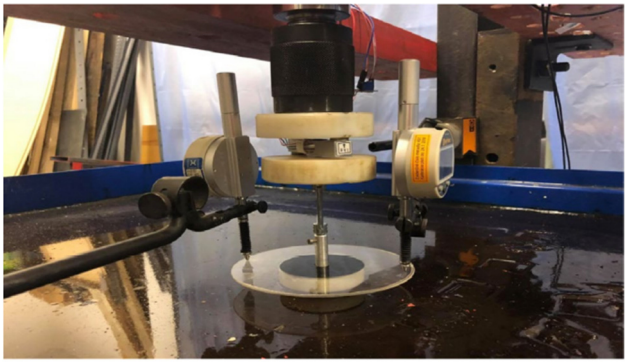

Fig. 2: Plate load test of simulation mass

Acknowledgements

This work was supported by Grant National Agency VEGA of the Slovak Republic. Project number G1/0009/2023.

References

[1] François, S.; Pyl, L.; Masoumi, H.R.; Degrande, G. The influence of dynamic soil–structure interaction on traffic induced vibrations in buildings. Soil Dyn. Earthq. Eng. 2007, 27, 655–674.

VSB TECHNICAL UNIVERSITY OF OSTRAVA | FACULTY OF CIVIL ENGINEERING

VSB-Technical University of Ostrava, Faculty of Civil Engineering
Vysoká škola báňská – Technická univerzita Ostrava, Fakulta stavební

22nd International conference / 22. mezinárodní konference

MODELLING IN MECHANICS 2024 / MODELOVÁNÍ V MECHANICE 2024

23. - 24. 5. 2024

Proceedings of extended abstracts / Sborník rozšířených abstraktů

Topics / Tematické okruhy

The conference is focused on the following topics /
Konference je zaměřena na následující tematické okruhy:

- development and application of numerical methods in mechanics / rozvoj a aplikace numerických metod v mechanice,
- methods used in extensive tasks dealing with mechanics of continuum / metody řešení rozsáhlých úloh mechaniky kontinua,
- numerical modelling of static and dynamic behaviours of concrete, brick, steel, timber and composite building structures / numerické modelování statického a dynamického chování betonových, zděných, ocelových, dřevěných a kompozitních stavebních konstrukcí,
- interaction between subsoil and building structures / interakce stavebních konstrukcí s podložím,
- influence of undermining on building structures / vliv poddolování na stavební objekty,
- loads and responses of structures in extreme conditions / zatížení a odezva konstrukcí v extrémních podmínkách,
- rehabilitation, reconstruction and reinforcement of load-carrying structures in buildings / sanace, rekonstrukce a zesilování nosných konstrukcí staveb,
- statics and dynamics of building structures / statika a dynamika stavebních konstrukcí,
- automation of engineering tasks / automatizace inženýrských úloh,
- mechanics of materials / mechanika materiálů,
- non-linear mechanics / nelineární mechanika,
- fracture mechanics / lomová mechanika,
- experimental verification of structures / experimentální ověřování konstrukcí,
- modelling of structures subject to heat, including fire resistance / modelování teplotně namáhaných konstrukcí včetně požární odolnosti,
- reliability and probability tasks in mechanics / spolehlivostní a pravděpodobnostní úlohy v mechanice,
- analysis of durability and sustainability of building materials and structures / analýza trvanlivosti a udržitelnosti stavebních materiálů a konstrukcí,
- the environmental and human impact of traditional and new materials / vliv tradičních a nových materiálů na životní prostředí a člověka,
- nanomaterials and 3D printing in construction / nanomateriály a 3D tisk ve stavebnictví.

Scientific committee / Vědecký výbor konference

(in alphabetical order / v abecedním pořadí)

Assoc. Prof. Bartlomiej Blachowski, Ph.D., Polish Academy of Sciences, Poland,

prof. Ing. Jiří Brožovský, Ph.D., VSB - Technical University of Ostrava, Czech Republic,

prof. Ing. Radim Čajka, CSc., VSB - Technical University of Ostrava, Czech Republic,

Ing. Michal Drahorád, Ph.D., Czech Technical University in Prague, Czech Republic,

doc. Ing. Jan Eliáš, Ph.D., Brno University of Technology, Czech Republic,

doc. Ing. Petr Frantík, Ph.D., Brno University of Technology, Czech Republic,

prof. Pratanu Ghosh, Ph.D., California State University, USA,

prof. Ing. Norbert Jendželovský, Ph.D., Slovak University of Technology in Bratislava, Slovak Republic,

prof. Ing. Jiří Kala, Ph.D., Brno University of Technology, Czech Republic,

prof. Ing. Zdeněk Kala, Ph.D., Brno University of Technology, Czech Republic,

Assoc. Prof. Eng. Jacek Katzer, Ph.D., University of Warmia and Mazury, Olsztyn, Poland,

doc. Ing. Jan Klusák, Ph.D., Institute of Physics of Material Academy of Sciences of the Czech Republic,

doc. Ing. Petr Konečný, Ph.D., VSB - Technical University of Ostrava, Czech Republic,

prof. Ing. Eva Kormaníková, Ph.D., Technical University of Košice, Slovak Republic,

doc. Ing. Kamila Kotrasová, Ph.D., Technical University of Košice, Slovak Republic,

prof. Ing. Juraj Králik, Ph.D., Slovak University of Technology in Bratislava, Slovak Republic,

prof. Ing. Martin Krejsa, Ph.D., VSB - Technical University of Ostrava, Czech Republic,

doc. Ing. Vít Křivý, Ph.D., VSB - Technical University of Ostrava, Czech Republic,

prof. Ing. David Lehký, Ph.D., Brno University of Technology, Czech Republic,

prof. Ing. Antonín Lokaj, Ph.D., VSB - Technical University of Ostrava, Czech Republic,

Assoc. Prof. Eng. Izabela Major, PhD., Czestochowa University of Technology, Poland,

Assoc. Prof. Eng. Maciej Major, PhD., Czestochowa University of Technology, Poland,

prof. Ing. Drahomír Novák, DrSc., Brno University of Technology, Czech Republic,

doc. Ing. Jaroslav Odrobiňák, PhD., University of Žilina, Slovak Republic,

prof. Ing. Stanislav Pospíšil, Ph.D., Institute of Theoretical and Applied Mechanics Academy of Sciences of the Czech Republic and VSB - Technical University of Ostrava, Czech Republic,

Assoc. Prof. Majid Movahedi Rad, Ph.D., Szechenyi University in Gyor, Hungary,

Assoc. Prof. Aleksandar Sedmak, Ph.D., University of Belgrade, Serbia,

doc. Ing. Stanislav Seitl, Ph.D., Brno University of Technology and Institute of Physics of Material Academy of Sciences of the Czech Republic,

dr hab. inż. Paweł Sikora, prof. ZUT, West Pomeranian University of Technology in Szczecin, Poland,

doc. Ing. Miroslav Sýkora, Ph.D., Czech Technical University in Prague, Czech Republic,

doc. Ing. Katarína Tvrdá, PhD., Slovak University of Technology in Bratislava, Slovak Republic,

prof. Ing. Miroslav Vořechovský, Ph.D., Brno University of Technology, Czech Republic.

Děkujeme partnerům Fakulty stavební
VŠB-TU Ostrava.

We thank the partners of the Faculty of Civil Engineering,
VSB-Technical University of Ostrava.

Title / Název:	Proceedings of extended abstracts **Modelling in Mechanics** 22nd International Conference 23rd and 24th May 2024 / Sborník rozšířených abstraktů **Modelování v mechanice** 22. ročník mezinárodní konference 23. - 24. 5. 2024
Author / Autor:	Team of authors / Kolektiv autorů
Place, year, edition / Místo, rok, vydání:	Ostrava, 2024, 1st edition / Ostrava, 2024, 1. vydání
Number of pages / Počet stran:	38
Published by / Vydala:	VSB-Technical University of Ostrava / Vysoká škola báňská – Technická univerzita Ostrava
Press / Tisk:	Editorial Center, VSB-Technical University of Ostrava / Ediční středisko, Vysoká škola báňská – Technická univerzita Ostrava
Number of copies / Náklad:	66

Not for sale / Neprodejné

ISBN 978-80-248-4735-1 (Print)

ISBN 978-80-248-4736-8 (Online)